AN INTEGRATED AC-DC RECTIFIER CONVERTER FOR LOW VOLTAGE PIEZOELECTRIC ENERGY HARVESTING AND CONSTANT-VOLTAGE LITHIUM-ION CELL CHARGING APPLICATION

Tasneem Rumman Huq

A Thesis

In the Department

Of

Electrical and Computer Engineering

Presented in Partial Fulfillment of the Requirements

For The Degree Of

Master of Applied Science (Electrical and Computer Engineering) at

Concordia University

Montreal, Quebec, Canada

May, 2015

CONCORDIA UNIVERSITY
SCHOOL OF GRADUATE STUDIES

This is to certify that the thesis prepared

By: Tasneem Rumman Huq

Entitled: "An Integrated AC-DC Rectifier Converter for Low Voltage Piezoelectric Energy Harvesting and Constant-Voltage Lithium-Ion Cell Charging Application"

and submitted in partial fulfillment of the requirements for the degree of

Master of Applied Science

Complies with the regulations of this University and meets the accepted standards with respect to originality and quality.

Signed by the final examining committee:

_____ Chair
Dr. R. Raut

_____ Examiner, External
Dr. W. Ahmed (MIE) To the Program

_____ Examiner
Dr. M. Z. Kabir

_____ Supervisor
Dr. S. Williamson

Approved by: _____
Dr. W. E. Lynch, Chair
Department of Electrical and Computer Engineering

_____20_____ _____
Dr. Amir Asif, Dean
Faculty of Engineering and Computer Science

ABSTRACT

An Integrated AC-DC Rectifier Converter for Low Voltage Piezoelectric Energy Harvesting and Constant-Voltage Lithium-Ion Cell Charging Application

Tasneem Rumman Huq

Energy harvesting is probably one the most sought after solutions that is being given attention to and has become of great importance for last few years. Due to advances in microelectronics and growing demand of autonomous devices, researchers have been working on harvesting energy from ambient sources such as solar, thermal, wind and kinetic energy. Also, growth of rechargeable battery technology has resulted in research in ambient energy harvesting for charging purposes. In this field, piezoelectric effect has been identified as a viable solution to address both low power applications and battery charging applications. Piezoelectric effect is described as the phenomenon of generating a voltage from a mechanical stress and vice-versa. Piezoelectric elements have been seen to offer outstanding performance in scavenging energy because of their high power density, which make them suitable for integrated micro-generators. Many vibration-based harvesting technology use piezoelectric transducers as AC power source. This work emphasizes on vibration based piezoelectric energy harvesting from a very low input voltage source. The main objective of the thesis is to design a power converter that can successfully rectify and boost piezoelectric AC voltages from a few hundred millivolts to a stable usable DC voltage without the use of a bridge diode rectifier circuit.

The thesis begins with the introduction to the concept of energy harvesting and piezoelectricity, followed by investigation of a 13x25 mm, 28µm thick, laminated piezoelectric thin film made of Polyvinylidene Fluoride (PVDF) acting as the transducer. The transducer was subjected to a repeated vibration impulse and its resultant voltage response was

determined. The thesis then moves towards presenting an integrated AC-DC rectifier converter which eliminates the use of full bridge diode rectifiers that have been known for being inefficient for low power energy harvesting. The stages of operation of the power converter is presented along with the simulation results. The work has also been extended to show the charging application of a Lithium-Ion thin film cell under constant voltage charging scheme using a MATLAB/SIMULINK battery model. A prototype of the converter was also built in the laboratory and presented to show the performance of the integrated AC-DC rectifier converter. A dSPACE controller board was employed to implement the open loop control and the converter switching scheme. Experimental results were presented and assessed before finally moving onto the conclusion and suggested future works.

ACKNOWLEDGEMENTS

The author would like to express his sincere gratitude to his supervisor, Dr. Sheldon S. Williamson, for introducing him to this project, and for his patient and invaluable guidance, advice and friendship throughout the author's Master's program.

The author would also like to thank his other distinguished professors and colleagues in the Power Electronics and Energy Research Group, at the P. D. Ziogas Power Electronics Laboratory for their valuable suggestions and friendship.

Special thanks to Dr. Najath Abdul Azeez for his support, friendship and unconditional help. Thanks to Dr. Muthukumaran Packirisamy and Dr. Jayan Ozhikandathil from the Optical Microsystems Lab for their support.

Last but not least, the author is grateful to his parents, Mrs. Mustary Begum and Mr. Khondoker Rumy Ehsanul Huq for their constant encouragement, love and support throughout his life.

TABLE OF CONTENTS

LIST OF FIGURES

LIST OF TABLES

NOMENCLATURE

AC	Alternating current
CC	Constant-Current
CCM	Continuous Conduction Mode
CMOS	Complimentary Metal-Oxide Semiconductor
CV	Constant-Voltage
DC	Direct Current
DCM	Discontinuous Conduction Mode
DSP	Digital Signal Processor
IADR	Integrated AC-DC Rectifier
Li-ION	Lithium Ion
MEMS	Microelectromechanical System
MOSFET	Metal Oxide Semiconductor Field Effect Transistor
Ni-Cd	Nickel-Cadmium
Ni-MH	Nickel Metal Hydride
Pb-ACID	Lead-Acid
PVDF	Polyvinylidene Fluoride
PWM	Pulse Width Modulation
PZT	Lead Zirconate Titanate

SoC	State of Charge
SSHI	Synchronized Switch Harvesting on Inductor

Chapter 1.

INTRODUCTION

1.1. Energy Harvesting

Ever-increasing consumption of fossil fuels has led to challenges like climate change, pollution and depletion of natural resources. With the progress of time, the demand of energy seems only to be increasing and has subsequently led to explore various other energy sources other than fossil fuels. Energy harvesting relates to the practice of capturing energy from ambient environmental sources. From the point of view of energy conversion, renewable energy sources have been utilized for decades and has steered the development of technologies like photovoltaic panels, wind generators, watermills and geothermal energy. These are examples of macro scale energy harvesting since renewable energy plants generate power in the levels of kilowatts to megawatts and most of the development lies in improving efficiency of the power systems eventually feeding into the electrical grid [1].

More recently, due to advancements in portable electronics, wireless sensor nodes and micro-electromechanical systems (MEMS), micro scale energy harvesting is also becoming the focus of academic as well as industrial research. The goal of this technology is to provide power in the ranges of microwatts to milliwatts to small, low power electronic systems, or to accumulate and store the energy for later use in storage devices like capacitors and batteries. Micro scale energy harvesting is typically based upon ambient environment such as mechanical vibration, stress and strain, thermal gradient, biological or chemical sources or even the human body.

1.1.1. Energy Harvesting Sources

A variety of energy harvesting sources are available including solar power, tidal waves, light energy, thermoelectricity and physical motions [2]. Some technologies used for energy harvesting are discussed below.

Solar Energy

Photovoltaic cells convert light energy into electrical energy and are quite popular as utilizing solar energy as a source of energy. Especially in the case of outdoor applications, solar photovoltaic panels have been shown to be promising for large scale energy harvesting. Solar energy has also been used for low power devices like watches and calculators as a secondary power source. However, energy harvesting technologies utilizing solar energy are affected by environmental factors such as light availability, latitude and intensity of light [3].

Wind Energy

Wind energy is perhaps considered as one of the most viable renewable energy sources. Windmills and wind turbine technology has shown dramatic progress over the last decade causing wind energy to become another promising source for large scale energy harvesting. In addition to harvesting wind energy in a large scale by wind farms, a few small scale wind energy harvesting research can also be found [4] [5].

Thermoelectric Energy

Thermoelectric generators convert thermal gradients directly into electrical energy through the Seebeck (thermoelectric) effect. The generated voltage and power is proportional to the temperature difference and the Seebeck coefficient of the thermoelectric materials [6] [7]. Solid state thermoelectric generators are considered to be reliable, long lasting and low maintenance. Although high temperature differences are

rare in micro-systems, resulting in low voltage generation, new thermoelectric generators are being developed for a variety of stand-alone, low power applications [2].

Vibration Energy

Mechanical vibration energy are ever-present in the environment, including machineries, civil structures or even human motion. Indoor machinery operating environments can provide constant mechanical vibration sources for vibration based energy harvesting [2].The area of vibration based energy harvesting encompasses mechanics, material science and electrical circuitry and include contributions from researchers from all three disciplines [8]. Vibration energy can be converted into electrical energy by either electromagnetic, electrostatic or piezoelectric techniques. Although the energy source is vibration, these three methods are very different to each other in terms of energy conversion methods and are described below:

- Electromagnetic: A magnetic field is utilized in this technique to convert mechanical to electrical energy. When an oscillating mass passes through a stationary permanent magnet, a voltage is induced due to varying magnetic flux according to Faraday's law.
- Electrostatic: This type of harvesting is based on a variable capacitance principle. A variable capacitor which is initially charged, separate its plates by vibration, changing the capacitance and extracting the electrical energy from the system.
- Piezoelectric: Piezoelectric microgenerators are the main focus of this thesis. Piezoelectric energy harvesting method is achieved by straining a piezoelectric material. These materials produce electric charge when strained by mechanical vibrations. Due to this ability to detect vibrations, piezoelectric materials have

become a viable energy harvesting source over the years and a topic of research for powering various applications.

1.2. Piezoelectricity

The term "Piezoelectricity" is derived from Greek meaning "pressure" electricity, and was discovered by the Curie brothers in 1880. They discovered that certain materials like quartz changed dimensions when they are exposed to electrical field. Conversely, these materials also generate charge when subjected to mechanical strain. This phenomenon was labeled as the piezoelectric effect.

1.2.1. Brief Description of Piezoelectric Theory

When a piezoelectric material is subjected to mechanical strain, either by tension or compression, it results in an induced voltage in the material. This is a result of the piezoelectric material getting electrically polarized due to the mechanical force. The charge can be attributed to the crystalline structure of the piezoelectric material. When a force is applied on piezoelectric materials, slight deformation in the atomic arrangement of the material gives rise to a charge density at the surface of the material which causes the material to become polarized. Electrodes placed on the surface of the material experience a voltage difference as a result of the induced field. Also it is important to note, when a piezoelectric material is mechanically strained, the electric polarization produced is proportional to the applied strain. This is called the "direct piezoelectric effect". When the same piezoelectric material is exposed to an electric polarization, it becomes mechanically strained that is proportional to the applied electric field, and it is called the "converse piezoelectric effect". The fundamental principles of piezoelectricity is well established and the IEEE Standard of Piezoelectricity [9] is the accepted standard describing the relationship and behavior of piezoelectric materials. Although the constitutive equations governing piezoelectricity are mostly expressed in tensor forms,

the relationship between displacement and electric field, and stress with strain, can be expressed in scalar forms given that the direction of the stress and the electric field are fixed, and are given by [10];

$$Direct\ Effect: \qquad D = \varepsilon.T + d.T \tag{1.1}$$

$$Converse\ Effect: \qquad S = d.E + s.T, \tag{1.2}$$

where, D is the electric displacement component (C/m^2), ε is the permittivity (F/m), d is the piezoelectric charge constant (C/N), T is the stress component (N/m^2), S is the strain component, E is the electric field component (V/m) and s is the elastic compliance constant (m^2/N).

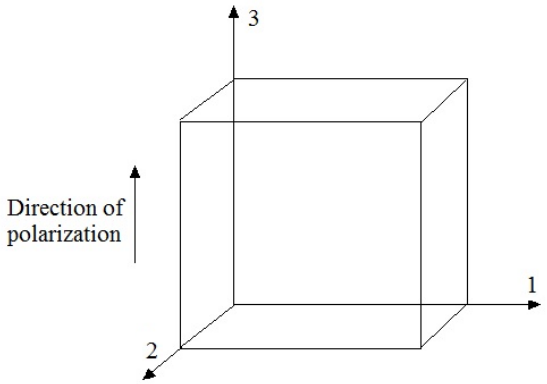

Fig. 1.1. Notation of axes system used to describe the properties of piezoelectric material

Piezoelectric materials usually exhibit anisotropic characteristics, meaning that the material properties differ depending upon the direction of forces and orientation of the polarization and the electrodes. The system of notations describing the anisotropic piezoelectric material is presented in Figure 1.1 [11]. The numbers 1, 2 and 3 refer to the orthogonal axes of a three dimensional coordinate system. By typical convention, the 3-direction refers to the direction of polarization. Two common modes of electromechanical

coupling are available when piezoelectric materials are used for energy harvesting purposes, the d_{31} and the d_{33} modes and is presented in Figure 1.2.

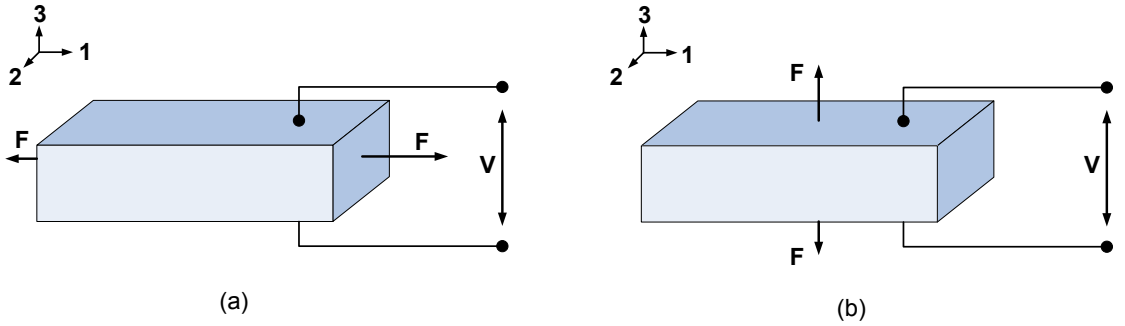

Fig. 1.2. Operating modes of piezoelectric materials (a) d_{31} mode (b) d_{33} mode

As mentioned before, d is the piezoelectric charge constant. The d_{31} mode is when the strain is applied in the 1 direction and the resultant electric potential is in the 3 direction. This is common in piezoelectric bending cantilever beams or films where the electric field is perpendicular to the mechanical strain. On the other hand, d_{33} mode is characterized by both the strain and the potential is in the 3 direction. Common example is piezoelectric stacks where both the strain and the electric field have the same direction.

1.2.2. Piezoelectric Energy Harvesting System

An overview of a typical piezoelectric micro-energy harvesting system is discussed in this section. A block diagram representation of the system is shown in Figure 1.3. Four main blocks or sub-systems form the complete energy harvesting system, the ambient vibration energy, piezoelectric transducer, the power converter circuit and the energy reservoir or the electrical load. Figure 1.3 also facilitates in understanding the flow of energy within the system. E_{ME} is the mechanical energy that acts upon the transducer, E_{IN} is the transformed electrical energy that is the input into the power converter, and the final harvested energy supplied to the load side is denoted as E_H.

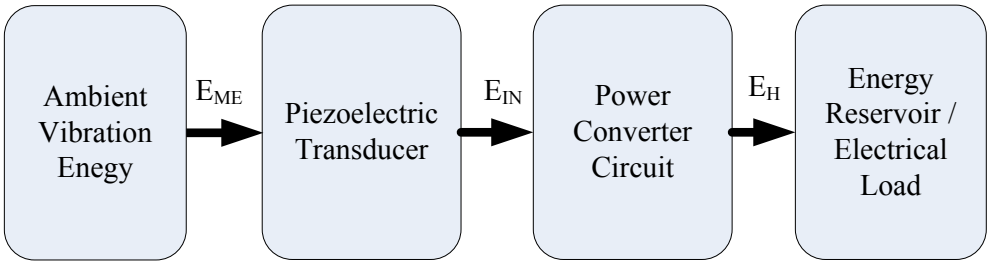

Fig. 1.3. Schematic representation of the concept of piezoelectric micro-energy harvesting system

The block for the ambient vibration energy represents the mechanical vibration that is intended to be used. When a piezoelectric material is generating charge upon being subjected to stress it is called piezoelectric transducer or generator. This characteristic can be used for sensor applications, such as accelerometer, microphones, or to harvest energy from environment. Most piezoelectric transducers used for energy harvesting are in the form of cantilevered beams. The transducer is positioned on a vibrating host structure or in a position where the vibration impulses act directly on the transducer itself. Under periodic vibrations, the transducer converts the mechanical energy into an alternating voltage output.

The resulting alternating voltage output from the transducer should be conditioned and converted into a stable rectified voltage for charging a small battery or to power a small load. The block for the power converter circuit consists of the relevant circuitry that performs this task. The power converter is an extremely crucial part of the system as it has to be designed keeping in mind both the input to the converter and the demand of the end application system. More on the relevant power electronic converters can be found in the literature review section.

In piezoelectric energy harvesting literature, some work can be found that focus on all the sub-systems together to address a complete system. Although, more often

research is done concentrating on one or some of the sub-systems concerning the aspects of the transducer or the power converter. This thesis will aim to concentrate on the middle two sub-systems, the piezoelectric transducer and the power converter. The scope of this research predominantly lies on designing the power converter circuit for piezoelectric energy harvesting purpose. However, it is a more concrete approach to investigate an appropriate transducer and its nature of output voltage that the power converter is required to rectify and regulate. Although battery charging is considered as the primary end application system it was not a subject of dominant focus in this research, nonetheless an introduction to energy storage is made in the next section.

1.3. Energy Storage for Energy Harvesting Applications

Energy storage technology is almost equally as diverse as energy harvesting, with many battery types available for storing the harvested energy from the many energy extracting mechanisms from environment [12]. Rechargeable batteries, known as "secondary" cells are suited and cost-effective for energy harvesting applications than "primary" or single-use cells. The most widely available batteries are Lead-acid (Pb-Acid), Nickel Cadmium (Ni-Cd), Nickel Metal Hydride (Ni-MH) and Lithium-Ion (Li-Ion). This section aims at acquainting with storage device parameters, particularly with Lithium-ion battery cells. Lithium-ion batteries have gained incredible popularity in recent years and can be found in almost all kinds of portable devices like laptops, cell phones, personal digital assistants (PDA's) and music players. The primary reason for this is the high energy density of Li-ion batteries.

1.3.1. Lithium-Ion (Li-Ion) Battery Cell

Lithium-ion batteries have high energy density, specific power and the potential for technological advancements compared to other battery chemistries. A typical 1 kilogram of Lithium-ion battery can store about 150 watt-hour of electrical energy.

Because of their high energy density they can be charged and discharged faster than Pb-Acid and Ni-MH batteries. Lithium-ion batteries are able to handle hundreds of charging and discharging cycles. Unlike other battery chemistries, they do not have to be completely discharged before recharging. Thin-film secondary cells are a specific class of Li-ion cell in which the reduced dimensions of the cell components increase the active surface area of the electrodes, thus allowing manufacturers to squeeze more active ingredients into a much smaller cell volume and resulting in dramatic increase in performance [13].

However, a weak point of Lithium based batteries is safety if not managed properly. Most Lithium-ion batteries have a charging voltage of 4.2 Volts. They can very easily absorb extra charge and explode if overcharged. Lithium-ion batteries need to be charged with a carefully controlled constant current or constant voltage regime to ensure reliable charging process.

1.3.2. Battery Parameters

Although the focus of an energy harvesting system designer might not be on cell structures and chemistries, it is important to have some brief working knowledge of the basic battery parameters. A brief definition of some basic battery parameters are given below [14].

Nominal Voltage & Cutoff Voltage

Nominal voltage of a battery is measured in Volts and is the specified reference voltage of the battery. It represents the end of the linear zone of the discharge characteristics. The cutoff voltage of a battery is the minimum specified voltage for operation. When the battery voltage reaches its cutoff voltage value, it is considered empty.

Battery Capacity

The battery capacity is usually measured in Ampere-hour (Ah) and indicates the amount of charge that a fully charged battery can supply until it reaches the cutoff voltage. It can simply be explained as the number of hours for which the battery can provide a current equal to the discharge rate at the nominal voltage of the battery.

State of Charge

State of charge (SoC) of a battery is the remaining battery capacity at a given point in time, expressed as a fraction of the maximum capacity. Therefore it is a good indication of the battery's charge level. Theoretically, state of charge value of 100 would mean the battery is fully charged. In practical scenario, state of charge of a battery is difficult to measure directly and usually some methods are used to make an indirect estimation of its value.

1.3.3. Charging Methods

Charging or recharging a battery in general means putting energy back into the battery. Different battery chemistries have different charging processes. The most common charging techniques for Lithium-ion batteries are described below [14].

Constant Current Charging

Constant current (CC) charging regime is charging the battery by applying a regulated constant current to the battery with low percentage of current ripples. In this phase of the charging process the battery cell is charged by the maximum charging rate recommended by the manufacturer. The rate is usually called the 1C rate and is equal to the ampere-hour rating of the cell.

Constant Voltage Charging

As suggested by the name “Constant Voltage” is when a constant voltage is applied to the battery. The applied voltage value is a pre-set value provided by the manufacturer depending on the battery type. For Li-Ion cells the value of 4.2V +/- 50mV is typically desirable. For effective charging to take place it is crucial to maintain the desired charging voltage since overvoltage can damage the cells and under-voltage might cause partial charging which over time reduces the life of the battery.

1.4. Literature Review

In order to achieve an effective piezoelectric energy harvesting system, the piezoelectric transducer must be interfaced with a power electronic circuitry that conditions the generated electrical energy into forms that is compatible for load electronics or a storage device. Most piezo transducers inherently produce AC voltage that require rectification. This section discusses a brief review of the literature of power converter topologies that have been implemented in piezoelectric based vibration energy harvesting.

The standard full bridge diode rectifier-capacitor circuit is the easiest way to rectify an AC voltage into a stable DC voltage, although the output is not regulated. The circuit presented by Ottoman et al. [15] consists of a full bridge diode rectifier, which consists of four diodes to rectify the sinusoidal input voltage, followed by a large capacitor that filters any non-DC components. The rectifier-capacitor circuit is then followed by a DC-DC converter that regulates that flow of energy into a battery. The subsequent two-stage rectification process is shown in Figure 1.4. In another work [16], they introduced an optimized step-down DC-DC converter that operated in discontinuous conduction mode (DCM). Step-down converter was considered assuming the piezoelectric transducer generates higher voltage levels than required by the battery.

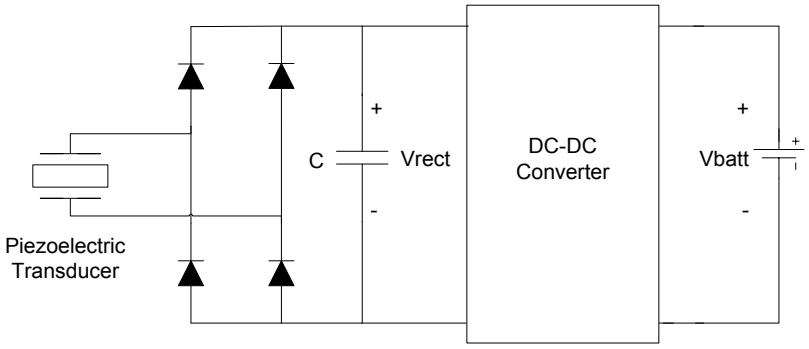

Fig. 1.4. Two-stage AC-DC rectification topology

Guan and Liao [17] summarized the optimized two-stage harvesting process introduced in [16] and provided an efficiency estimate for the step-down DC-DC converter and an improved estimate of the optimal duty cycle as well. In another work [18] they investigated the characteristics of several storage devices affecting the charging and discharging efficiency in piezoelectric energy harvesting systems.

Lefeuvre et al. [19] proposed using a sensor-less buck-boost converter running in discontinuous conduction mode after the rectifier in order to discover the optimal conditions for the energy harvesting system. A similar approach was taken by Kong et al. [20] to present a resistive impedance matching circuit by connecting a buck-boost converter operating in DCM right after the full bridge diode rectifier but eliminating the use of the smoothing capacitor in between the rectifier and the DC-DC converter.

Another converter topology based on the rectifier-capacitor circuit is the "Synchronized Switch Harvesting on Inductor" (SSHI) presented by Guyomar et al. [21]. The topology is similar to that of the standard rectifier-capacitor topology but with the addition of a switch and an inductor (connected in series) between the piezoelectric element and the rectifier. The technique is shown to increase the electromechanical conversion capability compared to the standard technique. Two different SSHI configurations have been developed by Badel et al. [22], the parallel SSHI where the

switch and the inductor are in parallel to the piezoelectric source and rectifier, and the series SSHI where the switch and the inductor are in series with the piezoelectric source and rectifier.

An approach using a bias-flip rectifier with an inductor was presented by Ramadass et al. [23] that improves the power extraction capability from piezoelectric transducer over conventional full bridge rectifiers and voltage doubler circuits. It consisted of a switch and inductor (connected in series) in parallel to the piezoelectric source and the rectifier circuit to reduce the losses associated with charging the source capacitance. The inductor used by the bias-flip rectifier was shared efficiently with a multitude of DC-DC converters to regulate the output.

A rectifier free piezoelectric energy harvesting circuit was suggested by Kwon and Rincon-Mora [24]. The circuit was shown to be scalable and consists of two switching converters operating in alternating cycles of the AC piezoelectric input. The suggested circuit uses only one inductor for both the converters as the low-loss energy transfer medium. Switching transistors were used to implement the diodes in the converter to reduce conduction losses. In another work, the scheme was developed and extended by them to store energy into storage devices with decent efficiencies [25].

For very low input piezoelectric voltage Peters et al. [26] suggested a two stage concept that includes a passive stage and only one active diode as second stage which result in rectification with high efficiency. The first stage used four standard CMOS transistors to convert the negative cycles of the sinusoidal input into positive ones. But the first stage itself is not able to retain the charge on the storage capacitor, hence in the second stage an active diode is used instead of a conventional diode which greatly reduces voltage drop.

1.5. Thesis Motivation and Contributions

Vibration energy is ubiquitous in nature and vibration based energy harvesting using piezoelectric materials has received significant attention due to their potential for converting the ambient energy into usable electrical energy. A piezoelectric energy harvesting system is a dynamic system consisting of source vibrations, transducer, energy harvesting circuitry and an end application system. The bridge rectifier circuit is the most commonly used electric interface for using the AC voltage generated by the transducer into DC, though the output is not regulated, hence leading to the use of other DC-DC converters following the rectifier. However, the main challenge is that this two-stage rectification process or the conventional diode bridge rectification is extremely inefficient for transducers producing very low voltage, due to voltage drops and associated losses in the diodes. Also, weak vibrations which result in low voltage output from transducers are also prevalent in environment. As seen from Section 1.4, bridge rectifier-free converter topologies and designs for low input are very limited. Therefore, well designed energy harvesting interfaces for low voltage sources are highly desired. The primary objective of this thesis is to design a functional single-stage power converter for piezoelectric energy harvesting that is able to extract the energy from the low AC voltage input, and step it up to a regulated DC signal that can be deposited in an energy storage device.

The major contributions of this research work are:

- Building a vibration test setup and carrying out experimental investigation on a Polyvinylidene Fluoride (PVDF) thin film piezoelectric transducer to determine the transducer output voltage range and resonant frequency of operation.
- Using the conclusions from the transducer behavior, proposing a single stage integrated AC-DC rectifier converter circuit for low input voltage operation.

- Performance verification of the proposed circuit topology, operation and demonstrating battery charging capability through simulations.
- Designing and building an appropriate pulse generator for the converter switching scheme implementation using dSPACE development system.
- Building a circuit prototype and experimental demonstration of the converter operation.

1.6. Thesis Outline and Structure

The contents of this thesis are organized in 5 chapters

Chapter 1 provides an overview of energy harvesting, piezoelectric theory and lithium-ion battery parameters. Literature review of the power electronic converter topologies and design concepts most widely used for piezoelectric energy harvesting is also discussed.

Chapter 2 of the thesis starts with an introduction to PVDF thin film transducer and its electrical equivalent circuit derivation, then proceeds onto describing vibrational tests conducted on the transducer and presenting the experimental results.

Chapter 3 introduces us to the proposed single stage integrated AC-DC converter circuit topology, its stages of operation, switching schemes and design considerations. Simulation results concerning converter performance and battery charging application is also presented.

Chapter 4 starts with the description of the constructed power circuit in laboratory in order to test the integrated AC-DC rectifier concept. The test bench setup and the employed apparatus is also presented. The dSPACE system implementing the switching

scheme is described. Experimental results concerning the dSPACE switching scheme and converter performance is also presented and assessed.

Chapter 5 summarizes the work carried out in this thesis and the final conclusions. Suggestions for future work on the topic are also presented.

Chapter 2.

STUDY OF POLYVINYLIDENE FLUORIDE PIEZOELECTRIC TRANSDUCER CHARACTERISTICS

2.1. Introduction

Piezoelectric materials are available in many forms like single crystals (e.g. quartz), piezoceramics (e.g. lead zirconate titanate or PZT), thin film (e.g. sputtered zinc oxide), screen printable thick film based upon piezoceramic powder [27] [28] and polymeric materials such as Polyvinylidene Fluoride (PVDF) [29]. When piezoelectric energy harvesting is considered, the material under consideration is an important choice and should be made based on not only the material's piezoelectric properties, but also its application, ease of operation and availability.

Table 2.1. Comparison of Common Piezoelectric Materials [30]

Property	**Units**	**PVDF Film**	**PZT**	**$BaTiO_3$**
Density	$10^3 kg/m^3$	1.78	7.5	5.7
Relative Permittivity	$\varepsilon/\varepsilon_o$	12	1200	1700
d_{31} Constant	$(10^{-12})C/N$	23	110	78
g_{31} Constant	$(10^{-3})Vm/N$	216	10	5
k_{31} constant	% at 1 KHz	12	30	21
Acoustic Impedance	$(10^6)kg/m^2$-sec	2.7	30	30

Some common piezoelectric material properties are presented in Table 2.1. The notation d_{31} has already been explained earlier in this thesis (refer to Section 1.2.1). The *g* coefficient gives an idea about the material's ability to produce voltage and the electromechanical coupling coefficient is represented by *k*. Although Table 2.1 demonstrates PZT and $BaTiO_3$ to have a higher piezoelectric constant and

electromechanical coupling factor, PVDF has a higher voltage generating capability compared to PZT and $BaTiO_3$. One of the main components of PZT is lead which is environmentally harmful. Also PZT is brittle in nature and unsuitable for application where forces directly act upon the material. PVDF is much more flexible and durable and more suitable for use as thin film piezoelectric transducers. Considering these factors, PVDF was chosen to be the main transducer material in this study.

2.2. PVDF Thin Film Cantilever Transducer

Generating a decent amount of usable electrical energy, Polyvinylidene Fluoride (PVDF) has been demonstrated as an effective energy harvesting source material in several research works [31-34]. PVDF is also commercially available as thin films which permit variety of applications. Piezoelectric films are flexible, lightweight, tough, available in various sizes and are becoming quite popular as they can easily be installed where bulk materials cannot. They can be directly attached to a host structure without disturbing its mechanical motion. Also, their thickness lie in the ranges of μm, making their presence hardly conspicuous. The low thickness of the films result a small cross-sectional area and subsequently resulting in relatively smaller forces creating larger stresses within the material. Thin film transducers are generally used in applications having low magnitude forces, but can be used for higher force applications as long as the transducer is in the elastic region of the material.

One of the most common designs of piezoelectric transducers are in the form of cantilevers. Cantilevers typically operate in d_{31} mode, and the simple beam-bending concept makes cantilever based transducers a popular choice for investigating vibration based energy harvesting. Cantilever based commercial PVDF thin film transducers are also available which can generate charge due to deformation caused by base excitation or impulse forces applied externally on the device.

The PVDF thin film piezoelectric transducer used in this research is the LDT0-028K piezo film sensor made commercially available by Measurement Specialties Inc. It is a 13x25mm flexible 28µm thick piezoelectric PVDF film, laminated to a 0.125mm polyester for robustness, and along with screen printed silver ink based electrodes. The structure and the physical dimensions of the transducer are shown in Figure 2.1 and Figure 2.2 respectively.

Fig. 2.1. LDT0-028K laminated PVDF polymer thin film [35]

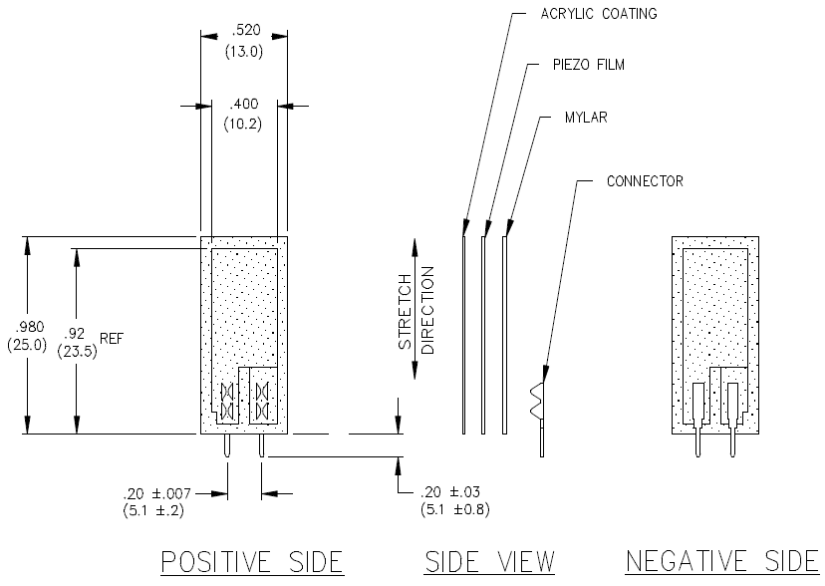

Fig. 2.2. LDT0-028K dimensions in mm [35]

Figure 2.3 shows a schematic representation of how the PVDF transducer film, or the piezo film in short, can be setup as a force-based cantilever type transducer. Force-based cantilevers are piezoelectric cantilevers that generates electric field when an

external force acts upon the cantilever. The piezo film is clamped to a rigid structure towards the end containing the electrodes and the rest of the film is allowed to remain suspended in free space.

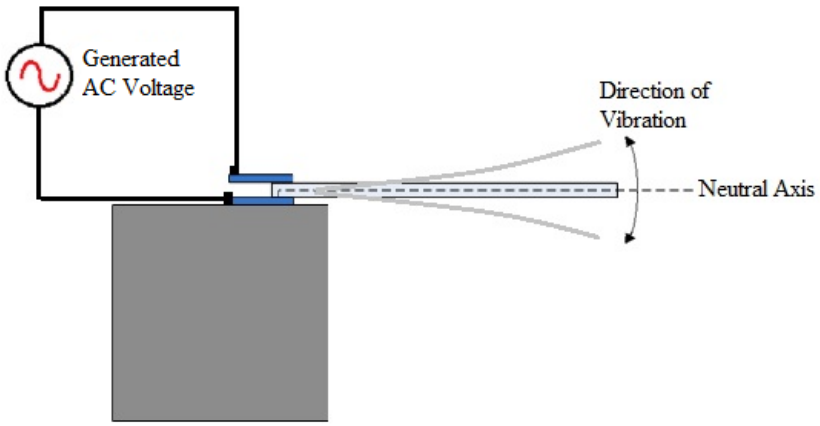

Fig. 2.3. Schematic of clamped PVDF piezoelectric film under stress producing voltage

When a force due to vibration causes the piezo film to displace from its neutral mechanical axis, the bending effect creates a strain on the film, therefore generating a charge which in turn causes a voltage to appear between the electrodes. The amplitude and the frequency of the voltage signal is directly proportional to the degree of mechanical deformation of the transducer. When the force is reversed, output voltage of opposite polarity is generated. Hence a reciprocating force results in an alternating output voltage from the transducer, as shown in Figure 2.3

2.3. Electrical Equivalent Circuit for Piezo Film Transducer

The thin film piezo transducer (or piezo film) used for converting the mechanical motion to electrical signals can be thought as a charge generator and a capacitor in parallel. This capacitor depicts the capacitance of the piezo film. Capacitance is a measure

of any component's ability to store charge and is always present when two conductive plates are brought close together. In this case, the conductive plates are the conductive electrodes printed onto each surface of the piezo film.

The capacitance of the material is strongly affected by the underlying properties of the insulator. Also, the measure of the material's ability to store charge is given by its dielectric constant or permittivity. Capacitance will increase as the area of the film increases and decreases as the thickness of the film increases. The factors related to the capacitance of the film can therefore be expressed as

$$C = \varepsilon \frac{A}{t} \tag{2.1}$$

where, C is the capacitance of the film, A is the active overlapping area of the film's electrodes, t is the film thickness and ε is the permittivity which can also be expressed as

$$\varepsilon = \varepsilon_r \varepsilon_o \tag{2.2}$$

where ε_r is the relative permittivity (which is about 12 for PVDF), and ε_o is the permittivity of free space (8.854 x 10^{-12} F/m).

The equivalent circuit diagram of the piezo film as a charge generator is presented in Figure 2.4. It shows a charge generator is parallel with the source capacitance C, and the leakage resistance R.

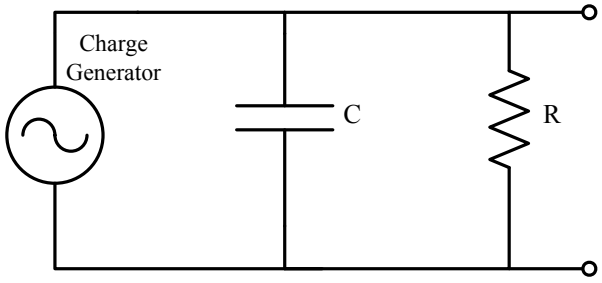

Fig. 2.4. Equivalent circuit for piezo film as charge generator

The magnitude of the induced surface charge is proportional to the applied force on the film. The value of the charge Q, in coulomb, generated across the capacitance and the leakage resistance is

$$Q = d.F \tag{2.3}$$

where, d is the charge sensitivity of the crystal (C/N) and F is the applied force (N).

The charge appears as voltage V across the electrodes of the piezo film acting as the transducer. The relationship between the induced charge and voltage can be described as

$$V = \frac{Q}{C} \tag{2.4}$$

Therefore the charge generator with the source capacitance in parallel can now be replaced by a voltage source in series with the capacitance. The value of leakage resistance is usually of very high range (in order of 10^{12} Ω) and hence its effect can be neglected and for the purpose of simplicity, not considered in this study. The equivalent circuit diagram of the piezo film as a voltage source is now presented in Figure 2.5.

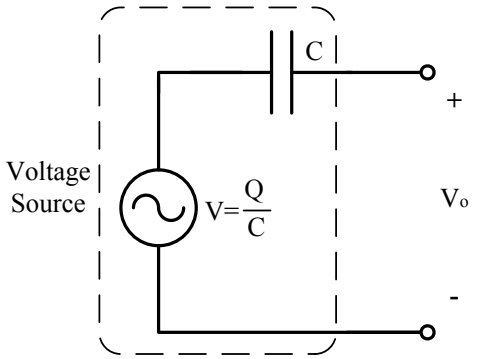

Fig. 2.5. Equivalent circuit diagram for piezo film as voltage source

The dashed line is used to represent the contents of the piezo film component. The voltage V is the piezoelectric voltage generated by the film itself and is directly proportional to the applied stimulus. However, an important note to be made is that the

film's capacitance C will always be present as an impedance when monitoring the output voltage V_o at the film's electrodes. Hence the output voltage V_o will always be smaller than the actual voltage V generated by the film due a voltage drop over the input impedance.

2.4. Loading Effect on Piezo Film Transducer

The first evaluation of the piezo film is done by connecting it up to a digital oscilloscope using scope probes. Usually a scope probe can be considered to have a very high (or infinite) impedance and its effect on the circuit is neglected. But this is not the case with piezoelectric films. Typical probes have an effective resistance of about 1MΩ. It should be noted that this physical element consisting of the effective resistance is usually built into the oscilloscope input stage. Hence connecting up the piezo film under test to a digital oscilloscope is equivalent to loading it up with a 1MΩ load. The circuit diagram is shown in Figure 2.6 with the oscilloscope and probe modelled as a resistive load R_L.

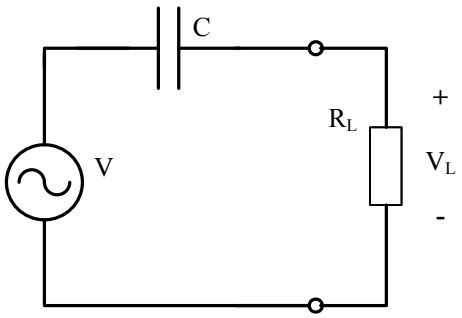

Fig. 2.6. Schematic diagram of the constructed power circuit

Taking a look at Figure 2.6, it is seen to depict a potential divider circuit and makes it easy to observe why the full source voltage does not appear across the resistive load. The capacitive element has an impedance that varies with the frequency and can be denoted as

$$Z_C = \frac{1}{jwC} \tag{2.5}$$

where w denotes angular frequency and j denotes √-1 (for capacitive reactance). The proportion of the source voltage V appearing across R_L can be given by

$$V_L = V\left(\frac{R_L}{R_L + Z_C}\right) \tag{2.6}$$

2.5. Experimental Investigation of PVDF Piezo Film Transducer

After presenting that the PVDF piezoelectric thin film is able to generate charge and voltage under stress, experimental tests were conducted obtain voltage values under real vibration conditions. The experiment would also be necessary to find the resonant frequency of excitation of the piezo-film where maximum voltage is produced. The experiment required a test setup and was built using electronics laboratory equipment that are commonly available like function generators, shaker and oscilloscopes. The vibration test setup is shown in Figure 2.7.

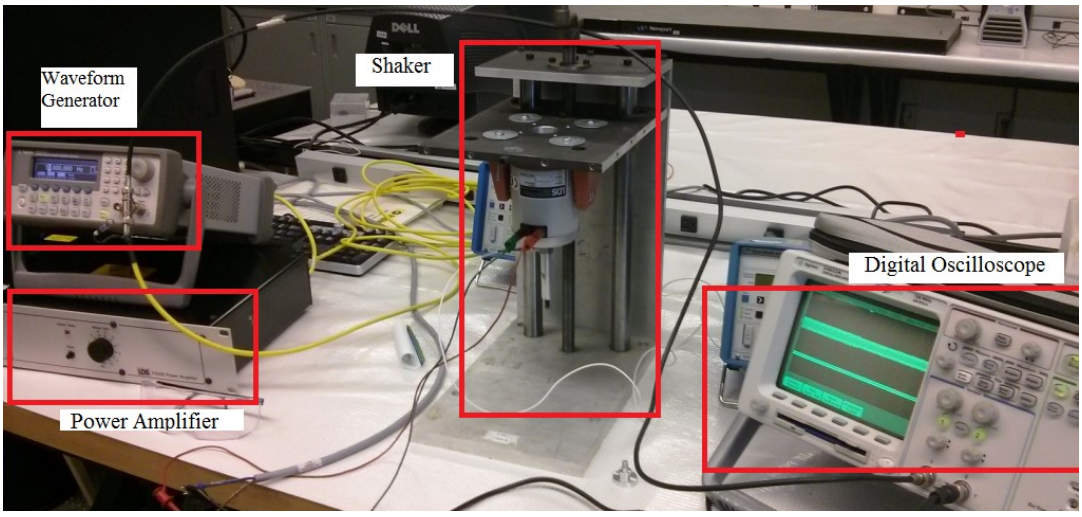

Fig. 2.7. Vibration test setup

Vibrational shakers are an easy way of simulating vibrations and very commonly used in literature also. LDS V203 permanent magnet shaker along with the LDS PA25E power amplifier was available at the Optical Microsystems Lab and is used for the purpose of vibration testing on the piezo-film. The LDT-028K piezoelectric film was mounted and clamped securely on a solid structure in order to keep it rigid so that impulse vibration could be applied on it through the shaker. Agilent 3320A arbitrary waveform generator was used to set a sinusoidal vibration to the shaker which would in turn provide an impulse to the piezo film. Agilent 54622A oscilloscope was connected to the output terminals of the piezo film to record and observe the nature of the transducer output voltage. Figure 2.8 shows the piezo film in place under the shaker. The extended knob from the shaker exerts the impulses to the piezo film in a way so that in each cycle of the exerted force the film bends from its neutral axis to give rise to an AC voltage at the electrodes.

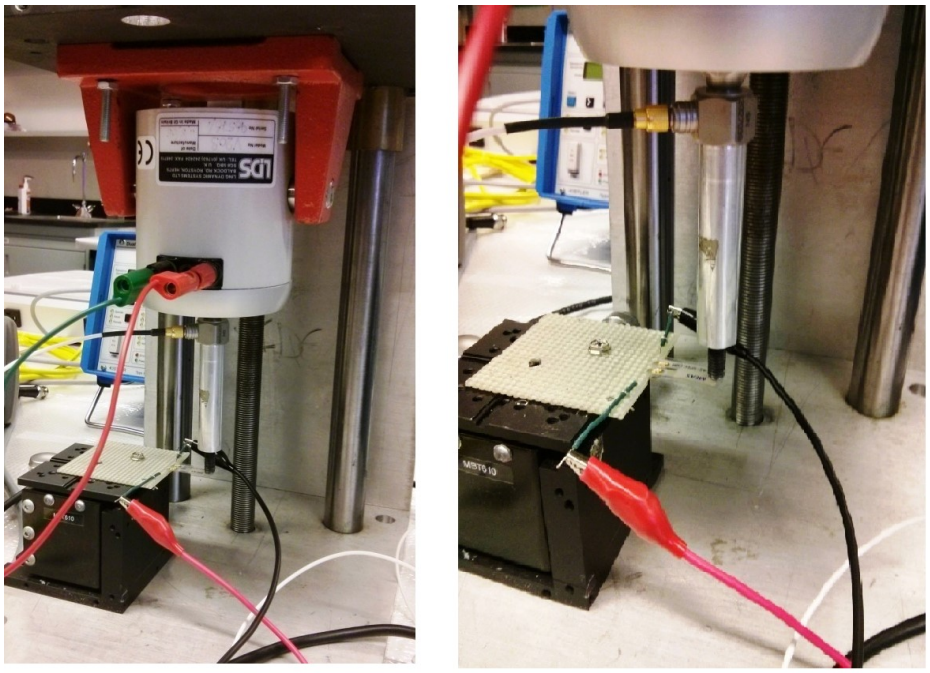

(a) (b)

Fig. 2.8. (a) Vibrational shaker and piezo-film in position (b) The piezo film under stress as the shaker is operating

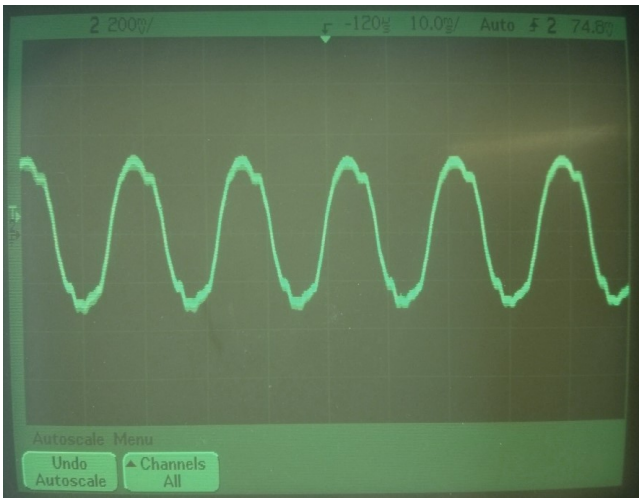

Fig. 2.9. Digital scope output from Piezo film under vibration

Figure 2.9 shows the direct output from the digital oscilloscope connected across the electrodes of the PVDF piezoelectric transducer that is under constant mechanical force due to the a constant vibration of the shaker, and confirms the AC nature of the resultant output signal from the transducer.

2.5.1. Resonant Frequency and Transducer Output Voltage Determination

Cantilever based piezoelectric transducers usually have a particular value of frequency of excitation where the transducer voltage output is at maximum. It is the frequency of oscillation at which the piezoelectric material is able to convert the mechanical energy into electrical signals with maximum efficiency. From an electrical point of view it is the frequency at which the transducer input impedance is at minimum. This is called the resonant frequency of the piezoelectric transducer or sensor. The resonant frequency is strongly dependent on the piezoelectric material and geometry, but it can also be tuned based on its mounting. Altering the free length of the element by clamping can change the resonant frequency. Applications where very low frequency of

excitation is used, small masses are often added to the tip of the cantilever to increase sensitivity at lower frequencies [35].

The first step in determining the resonant frequency of the piezo film in the experimental setup as described in Section 2.5 is to gradually increase the frequency of excitation of the shaker from a minimum value without changing the amplitude of the sinusoidal vibration and monitor the transducer output voltage. The output voltage should also increase gradually with increase in frequency and reach a maximum value at a certain frequency. As the frequency of excitation is increased beyond that value, the output voltage should drop again.

Figure 2.10 presents the experimental results when the peak value of the AC voltage (the output from the transducer) is plotted against frequency of vibration of the piezo film. As expected, it is seen that initially with an increase in frequency of vibration there is an increase in output voltage, the rate of increase in voltage increases rapidly as it approaches a certain frequency and gives a peak voltage value at about 45 Hz. The voltage amplitude then begins to fall with further increase in frequency of vibration. Hence it can be said that the resonant frequency in this case is 45 Hz and it implies that using any other frequency of excitation will result in inefficient energy conversion and much lower output voltage from the transducer. Besides ambient vibrations, this frequency of vibration excitation is also close to certain industrial and process environment vibration frequency level (of about 50 Hz) where vibration energy harvesting research is done [36].

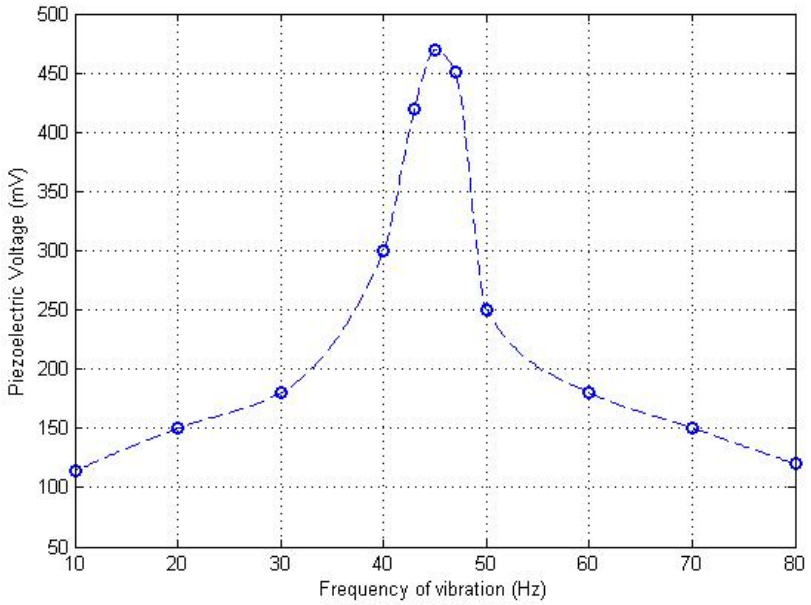

Fig. 2.10. Frequency response of piezoelectric transducer film

Once the value of the resonant frequency is determined experimentally, it is also necessary to acquire the range of output voltage amplitudes that the setup is able to generate from the vibrations. As mentioned in Section 2.2 the output voltage of the transducer is directly proportional to the applied stimulus or magnitude of stress experienced by the piezo film. Using the waveform generator to vary the amplitude of impulse by the shaker, the piezo film was subjected to several different magnitudes of force to monitor the variation of the corresponding output voltage response.

Figure 2.11 shows the transducer output voltage for different amplitudes of excitation. During experiments it was found that for each frequency of vibration, the highest voltage is generated from the highest amplitude of applied stress or vibration. Also it is observed that the peak amplitude of output voltage for each force level occur at around 45 Hz of frequency of vibration.

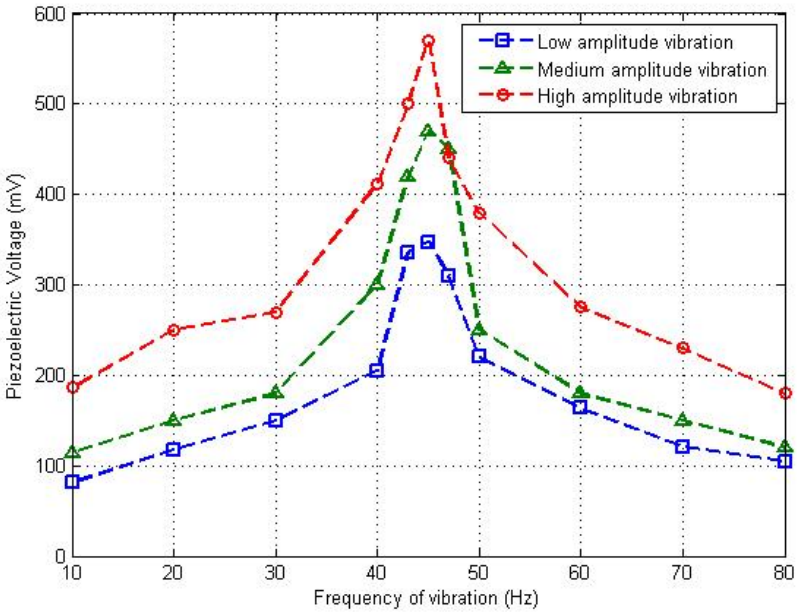

Fig. 2.11. Piezoelectric transducer output voltage relationship with frequency of vibration

This again confirms that the resonant frequency of the transducer is 45 Hz. The peak amplitude of output voltage from the piezo film transducer is found to range from about 350-600 millivolts when subjected to stress caused by the vibration of the shaker. These results play an important role in understanding the nature of the input voltage that a power conditioning converter can expect from the transducer. The amplitude of the converter AC input voltage would be ranging from about 300-600 mV with a frequency of 45 Hz (due to resonant frequency).

2.6. Summary of Chapter 2

This chapter provides a background on PVDF material and its role characteristics as a piezoelectric transducer. Theoretical development of the electrical equivalent circuit of the transducer as a charge generator and a voltage source is discussed. The chapter also includes a vibration test setup used to emulate a constant vibration environment. Testing the PVDF transducer under constant periodic vibrations demonstrate the voltage output

range of a microgenerator. Resonant frequency value at which transducer output is maximum is also experimentally determined.

Chapter 3.

POWER CONVERTER FOR LOW-VOLTAGE PIEZOELECTRIC ENERGY HARVESTING

3.1. Introduction

All energy harvesting applications require a suitable power electronic converter to process the input energy and deliver it to a load or store it in an energy storage device like capacitor or battery. The converter should take into account the nature of input from the transducer and the requirement of the load. If the input of the energy harvesting scenario is an AC source and the load requirement is DC then a rectifying circuit must be implemented.

As mentioned earlier, piezoelectric transducers when subjected to periodic vibration generates an alternating voltage which must be rectified to be useful for an electronic device. The harvester circuit must be able to extract the energy from the alternating voltage and deposit charge in an energy storage device. The easiest means of achieving this is to use a full bridge diode rectifier circuit. In fact most piezoelectric energy harvesting converters implement a two stage power converter using a full bridge diode rectifier circuit to rectify the AC input voltage, followed by a DC-DC converter to achieve the desired output voltage (refer to Section 1.4). Conventional diode bridge rectification is very inefficient for scenarios with low-voltage sources due to diode forward voltage drops. And yet, not much has been done in the field of piezoelectric energy harvesting taking into account input in the range of a few hundred millivolts. Hence the need to look into a single stage AC-DC rectifying converter circuit arises.

3.2. Integrated AC-DC Rectifier Converter

The proposed integrated AC-DC rectifier converter, henceforth addressed as IADR converter and presented in Figure 3.1, has been developed with the objective to eliminate the use of a diode bridge rectifier and its resulting losses, and to successfully step-up few hundreds of millivolt range voltage input into a usable voltage output level. However, few assumptions have been made in order to develop the IADR converter. The AC voltage source of the converter which is the input from the piezoelectric transducer has been assumed as an ideal voltage source whose peak is dependent on the amplitude of exciting vibration applied. Also the power delivered on the load side is dependent on the load of the converter itself.

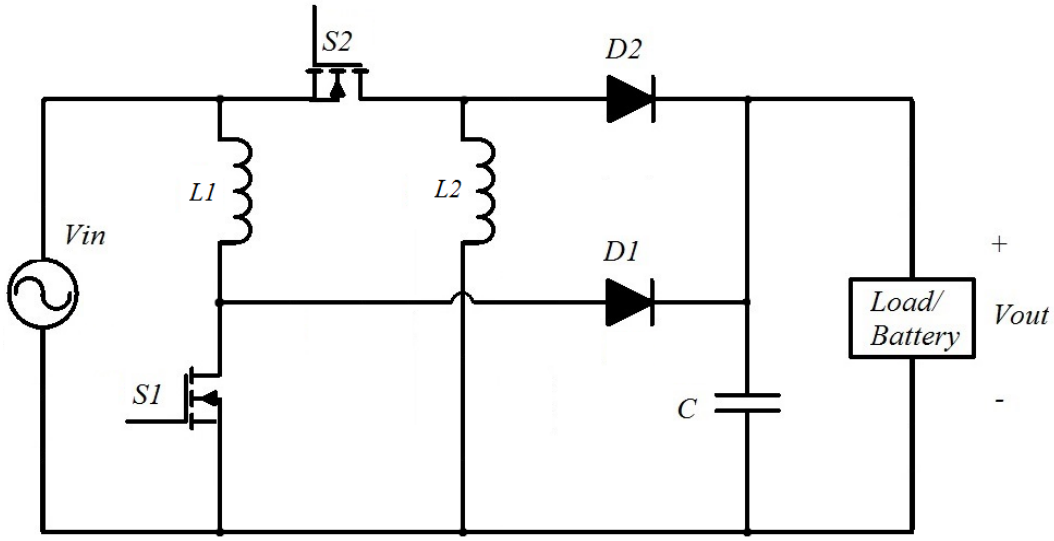

Fig. 3.1. Integrated AC-DC Rectifier Converter

Figure. 3.1 above shows the proposed IADR converter circuit. It can be classified as from being amongst the family of dual-polarity converters operating as one single converter [24] [37]. The IADR converter combines two separate DC-DC converters, a boost and an inverting buck-boost converter together in parallel. Since the

aim is to develop a step-up converter, both boost and buck-boost converters are ideal for the operation. The AC voltage input V_{in} is the voltage generated by the piezo film transducer. The principle is that the two converters will operate independently during each half cycle of the AC input voltage cycle and deliver a rectified voltage to the load side during both the positive and negative input cycles.

The boost converter is comprised of the harvesting inductor L_1, switch S_1 and diode D_1. The inverting buck-boost converter comprises of the second harvesting inductor L_2, switch S_1 and diode D_2. The boost converter operates only during the positive half cycle of the input voltage V_{in}, and the buck-boost converter operates only during the negative half cycle. It can be noted that although the direction of the diode D_2 has been reversed compared to the conventional buck-boost converter topology, the converter still retains properties of a buck-boost converter, and now ensures that the polarity of the output voltage during both the half cycles remains the same.

3.3. Converter Stages of Operation

The IADR converter has mainly four stages of operation. Two stages each for the boost and the buck-boost converter. The operating stages cover one entire cycle of source voltage. Stage 1 and Stage 2 are for the boost converter operating during the positive half cycle of the input voltage. Stage 3 and Stage 4 are for the negative half cycle of the input voltage when the buck-boost converter is operating. It is important to realize that during the boost converter operation only the switch S_1 operates at the switching frequency and switch S_2 is off. Similarly during the inverting buck-boost operation the switch S_2 is operating at switching frequency while S_1 is off. The switching scheme of the IADR converter is shown in Figure 3.2.

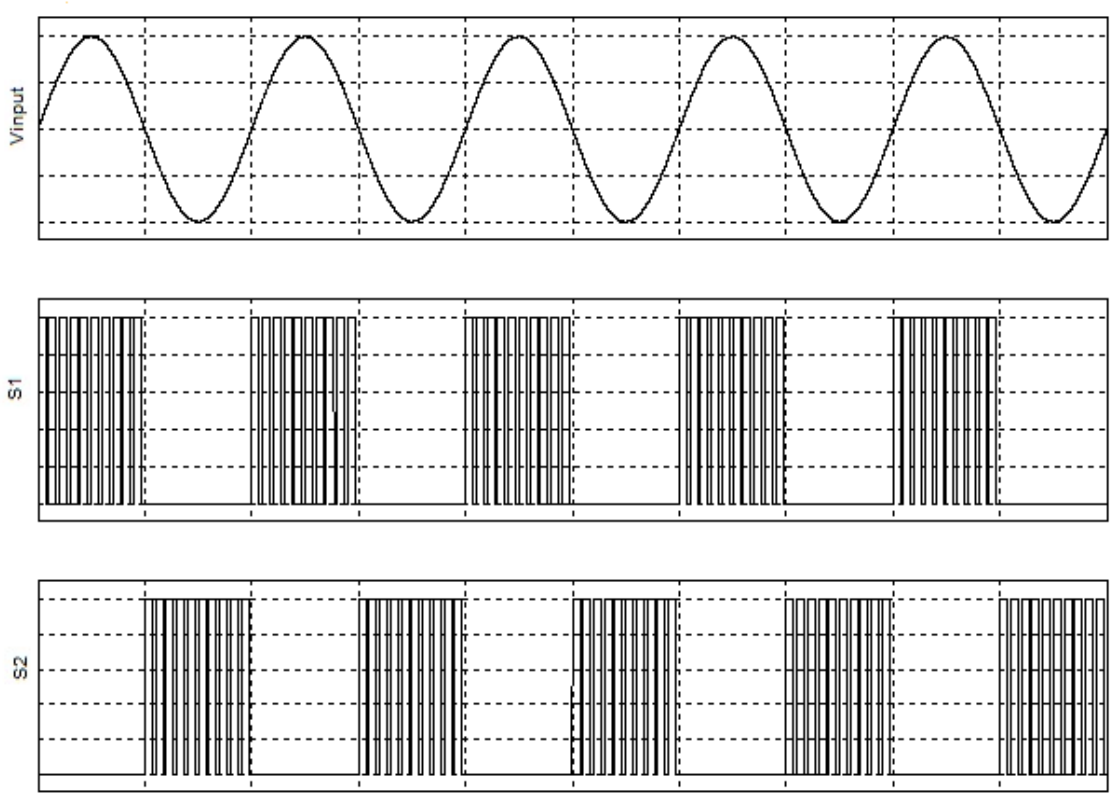

Fig. 3.2. Input voltage and gate pulses of switches S1 and S2

Figure 3.2 shows the IADR converter switching scheme over a few input voltage cycles. The boost converter switch S_1 operates only during the positive input cycle and the buck-boost converter switch S_2 operates only during the negative half cycle. This switching cycle is important for the functioning of the IADR converter as will be shown in its stages of operation.

3.3.1. Stage 1

Stage 1 operation starts at the beginning of the positive half cycle of the input. The boost converter's switch S_1 is turned ON and starts to conduct, this reverse biases the diode D_1, hence remaining OFF. The inductor L_1 starts building current i_{L1}. In this condition the diode D_2 and switch S_2 are also in OFF condition. Fig 3.3 below shows the operation of the IADR converter during stage 1.

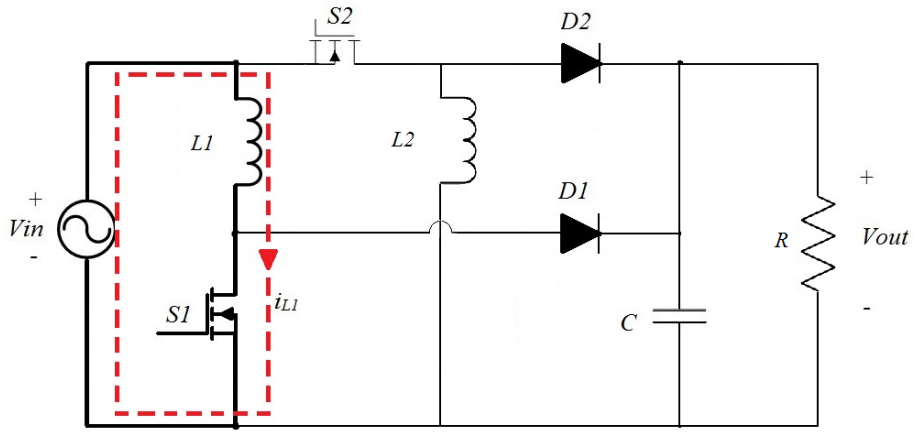

Fig. 3.3. Stage 1 operation of the IADR converter

3.3.2. Stage 2

Stage 2 operations starts at the end of stage 1 but still in the positive half cycle of the input. Boost switch S_1 is turned OFF which forward biases the diode D_1. This results in the inductor current i_{L1} now to flow through D_1 and charge the output capacitor C. The voltage across the capacitor is the output voltage across the load R. Switch S_2 and diode D_2 are still OFF. Fig 3.4 shows the operation of the IADR converter during stage 2.

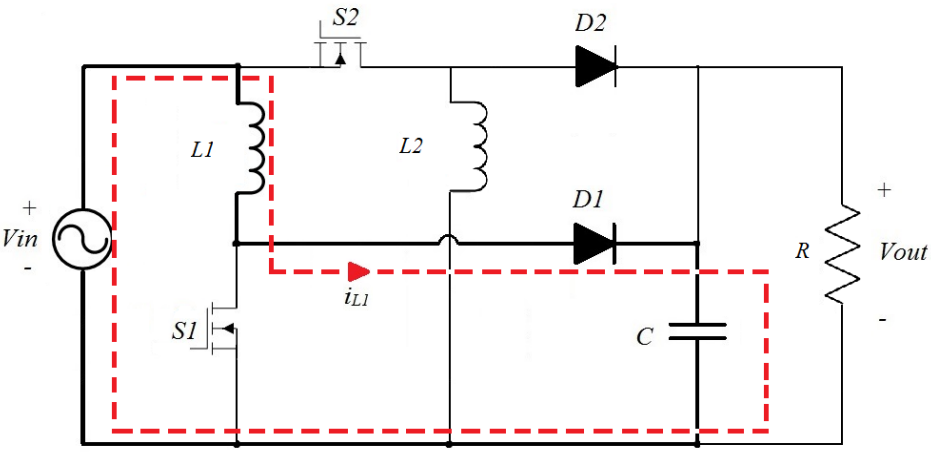

Fig. 3.4. Stage 2 operation of the IADR converter

3.3.3. Stage 3

Stage 3 starts at the beginning of the negative half cycle of the input. The buck-boost converter's switch S_2 is turned ON and the inductor L_2 starts building current i_{L2}. The diode D_2 is not conducting since it is reverse biased. Switch S_1 and diode D_1 are both OFF. Fig 3.5 below shows the operation of the converter during stage 3.

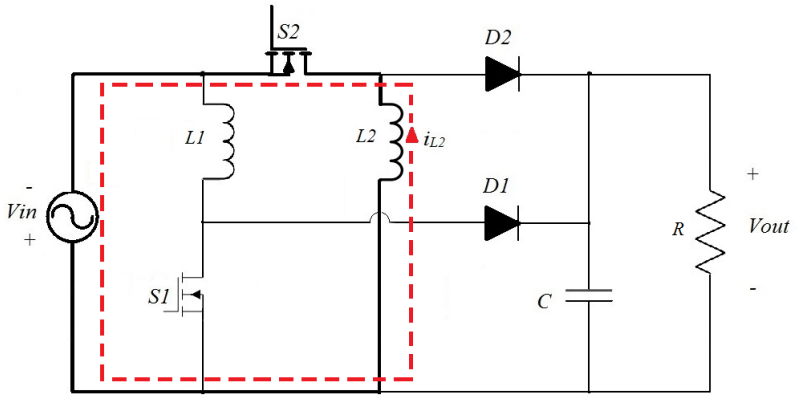

Fig. 3.5. Stage 3 operation of the IADR converter

3.3.4. Stage 4

Stage 4 is the last stage of operation. Switch S_2 is turned OFF, forward biasing the diode D_2. Inductor current i_{L2} now starts to flow through diode D_2 and charge the output capacitor C. The voltage across the capacitor is the output voltage across the load R. Switch S_1 and diode D_1 are both OFF.

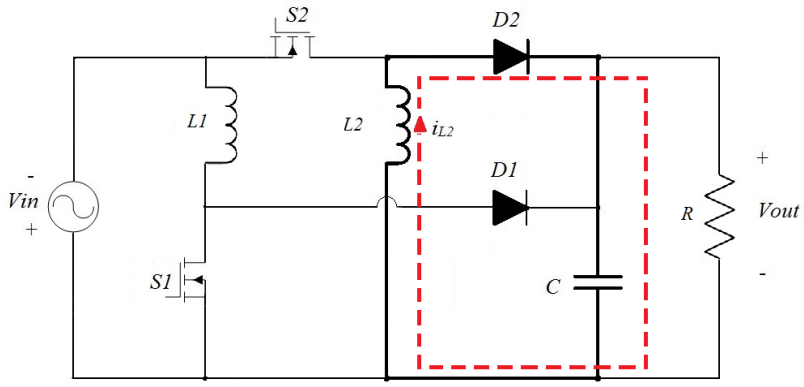

Fig. 3.6. Stage 4 operation of the IADR converter

From the stages of operation of the IADR converter, the basic operation of the converter operating over one entire input cycle can be perceived. Also, it is important to note that although the Schottky diode forward threshold voltage is almost equal to the input voltage amplitude, following the stages of operation where the inductors L_1 and L_2 build up current, the inductor voltages become high enough to easily overcome the threshold voltage of the diodes. Therefore, the converter successfully utilizes both the positive and negative cycles and supplying the load with the required voltage over both the input high cycle without using a separate rectifier circuit.

3.4. Design Principle

The main objective of the IADR converter is to step up and deliver a usable DC voltage from a very low AC input source. Therefore, the key design consideration to be given thought is to minimize the losses and voltage drops in the circuitry itself. Parasitic losses can never be fully eliminated and can have a huge impact especially in such lower power energy harvesting scenarios.

The forward threshold voltage of a typical p-n junction diode is around 0.7-0.8V under normal room temperature conditions. Diode forward voltage drop during diode conduction can prove to be very significant in terms of loss during the low voltage energy harvesting considered in this work. Hence Schottky junction diodes, or more commonly known as simply Schottky didoes, have been considered in this application. With a lower forward threshold voltage of about 0.3V, Schottky diodes promise to act as the favorable rectifying element in this work.

Another major aspect to consider in terms of the converter operation is whether to operate the IADR converter in continuous conduction mode (CCM) or discontinuous conduction mode (DCM). For low power applications like this, DCM mode has been

identified as the more efficient mode and has been used in practice [16] [38] [39]. Major advantage of DCM in this application is that it reduces switching losses which are significant in such low power application. DCM is often used in order to avoid the reverse recovery effect of the diode [16] [40]. Based on these criterions, the DCM mode of operation was chosen and implemented.

Although high switching frequency is useful in power converters as the inductor has to store less energy, very high switching frequencies will result in more switching losses due to hard switching. Also, switching frequency has a direct effect on the circuit current as will be shown below. For the purpose of simplicity, duty cycle of the boost and inverting buck-boost converter are both kept the same in this study.

Inductor sizing will play a crucial role in not only ensuring that the power converter is operating in the desired mode of operation, which is DCM in this case, it will also control the amount of current flowing through the circuit. From Fig. 3.1, it is evident that the inductor current is the input current in the converter during both the positive and negative voltage input cycles. Since the input voltage in each cycle is not constant but varying, the input current will also be following the input voltage profile and the peak inductor current will occur when the input voltage reaches its peak value V_{pk}. The peak value of the current I_{pk} can be found by [38]

$$I_{pk} = \frac{V_{pk}D}{Lf_s} \tag{3.1}$$

where L is the value of the inductors, f_s is the switching frequency and D is the duty cycle of the converters. Hence if the peak voltage and duty cycle is fixed, from Equation 3.1 it is clear that the peak current depends on the size of the inductor and clock parameters.

This peak inductor current is also the peak current through the switches hence the switch current rating can also be determined using this.

Low loss n-channel metal oxide semiconductor field effect transistor (MOSFET) are used to realize the unidirectional switches in the converter. Low on state resistance of MOSFET can also improve the performance of the converter. It can be noted that the forward voltage drop of the MOSFET body diodes are being utilized in the IADR converter topology. The switches S_1 and S_2 both encounter a reverse voltage during their OFF state due to the sinusoidal nature if the input voltage. But this reverse voltage conduction is blocked by the MOSFET body diode forward threshold voltage. This also places a limitation that this IADR converter topology will only work as long as the MOSFET body diode forward voltage is higher than the peak voltage V_{pk} of the input voltage. This limitation can be addressed by connecting two n-channel MOSFETs in series with back to back body diodes to emulate a four quadrant switch [25]. However, this series connection of two switches would increase the conduction and switching losses, which cannot be afforded in such low power application. Hence for this particular work, where the peak input voltage level V_{pk} is always lower than the MOSFET body diode forward voltage, the IADR converter topology's functionality is not compromised.

Another observation is that although the IADR topology is using two switches, two inductors and two diodes, each is being used for only one half cycle of the input cycle. Therefore considering both the positive and negative input cycles, it is like using one single switch, inductor and diode over one entire input cycle. Hence the inductor, switching and diode losses associated are also that of operating just one of each components.

3.5. Simulation Results

In order to verify the operation and test the performance of the IADR converter, open loop simulations were carried out. These simulation results would be important in determining if the converter is able to boost up the low AC input voltage to a higher, more usable DC voltage.

3.5.1. Open Loop Simulations

In this study the piezoelectric transducer is producing a sinusoidal AC voltage of about 300-600mV amplitude level and a frequency of 45Hz. The input frequency of 45Hz is the resonant frequency of vibration being applied to the piezoelectric film. The initial simulation parameters are listed in Table 3.1 below

Table 3.1. Description of Simulation parameters

Input Voltage, V_{in}	400 mV
Input Frequency	45 Hz
Switching Frequency, f_s	10 kHz
Inductor L_1	40 µH
Inductor L_2	40 µH
Output Capacitor, C	300 µF
Load Resistance, R	500 Ω
Schottky Diode D_1 Forward Voltage Drop	0.3 V
Schottky Diode D_2 Forward Voltage Drop	0.3 V
MOSFET S_1 and S_2 R_{ds} on	40 mΩ
Duty Cycle	0.7

Figure 3.7 shows the piezoelectric transducer input voltage and the corresponding IADR converter inductor currents. From the converter topology in Section 3.2, it is clear that the inductor currents are the input currents in the converter. The boost converter is

only building inductor L_1's current (in red) during the positive cycle and the buck-boost converter is building the inductor L_2's current (in blue) during the negative cycle. Therefore each inductor is building current in either the positive or negative cycle only, showing that the IADR converter is operating as desired. Also the currents are seen to be completely in phase with the input voltage cycle.

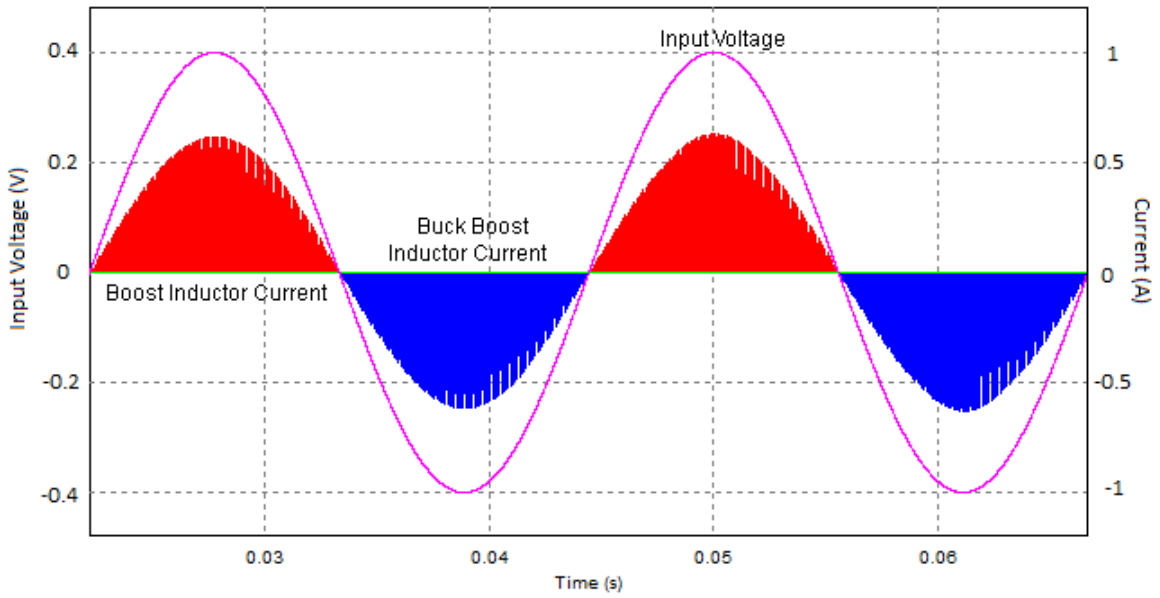

Fig. 3.7. Transducer input voltage and the inductor currents

Each switching cycle consists of the respective inductor current rising steadily when the switch is on, and then falling sharply when the switch is off, and remaining at zero until next switching cycle (since DCM mode). The peak of the inductor currents are also proportional to the input voltage as seen in Figure 3.7.

A closer look at the inductor currents I_{L1} and I_{L2} is shown in Figure 3.8. Figure 3.8 (a) shows the current I_{L1} flowing through the inductor L_1 during six switching cycles. The DCM mode of operation is evident from the figure. The same trend is seen for the current I_{L2} flowing through inductor L_2. Figure 3.8 (c) show the two inductor currents during a

zero cross-over period when the IADR converter switches from the boost mode to the buck-boost mode.

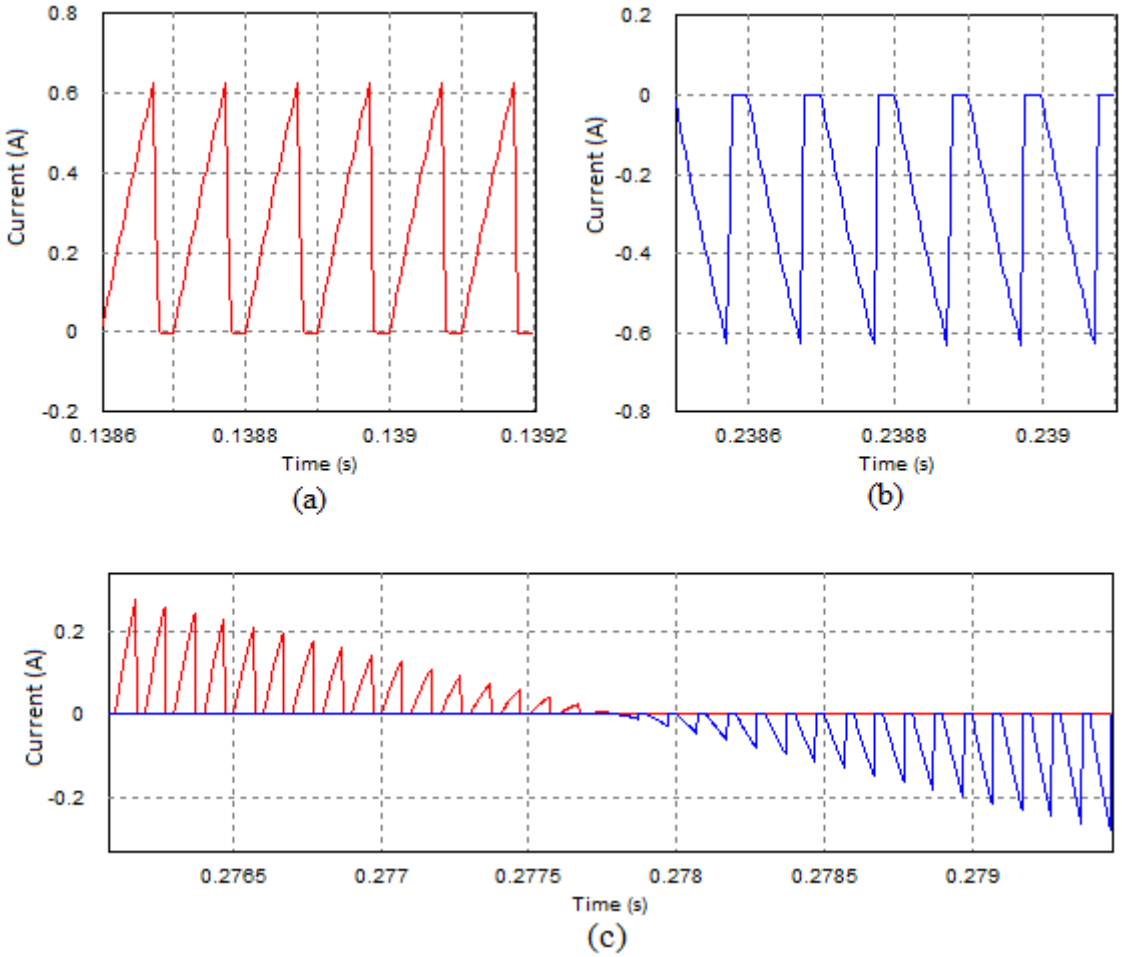

Fig. 3.8. Inductor currents (a) Inductor L_1 current, I_{L1} (b) Inductor L_2 current, I_{L2} (c) Inductor currents during a zero cross-over period

The IADR converter DC output voltage for the same parameters are shown in Figure 3.9. As the converter begins its operation, it charges the output capacitor during both the input half cycles and the capacitor voltage begins to increase from zero with each cycle until it reaches a steady output voltage. The figure above shows the output voltage after it has reached the steady state. The output is about 4.2V from an AC input voltage of 400mV, a step-up ratio of about 10 times.

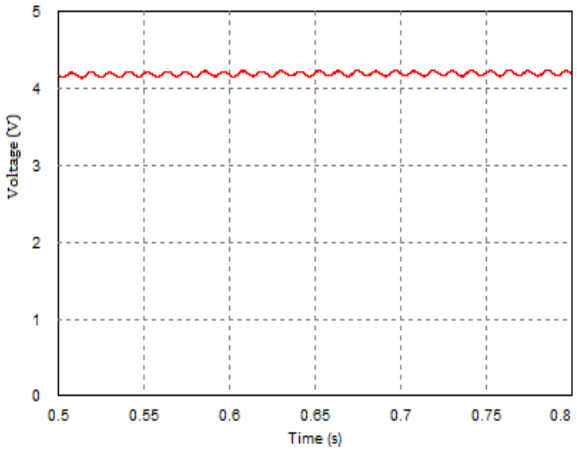

Fig. 3.9. Output voltage after reaching steady state

In order to compare the performance of the IADR converter with its two constituent fundamental converters (boost and buck-boost) in terms of output voltage, the same simulation was carried out separately for the three converters. The boost converter was made to operate during the positive half cycle and the buck-boost converter was made to operate during the negative half cycle only. The IADR converter was operating during both positive and negative cycle like it is supposed to. The results are presented in Figure 3.10.

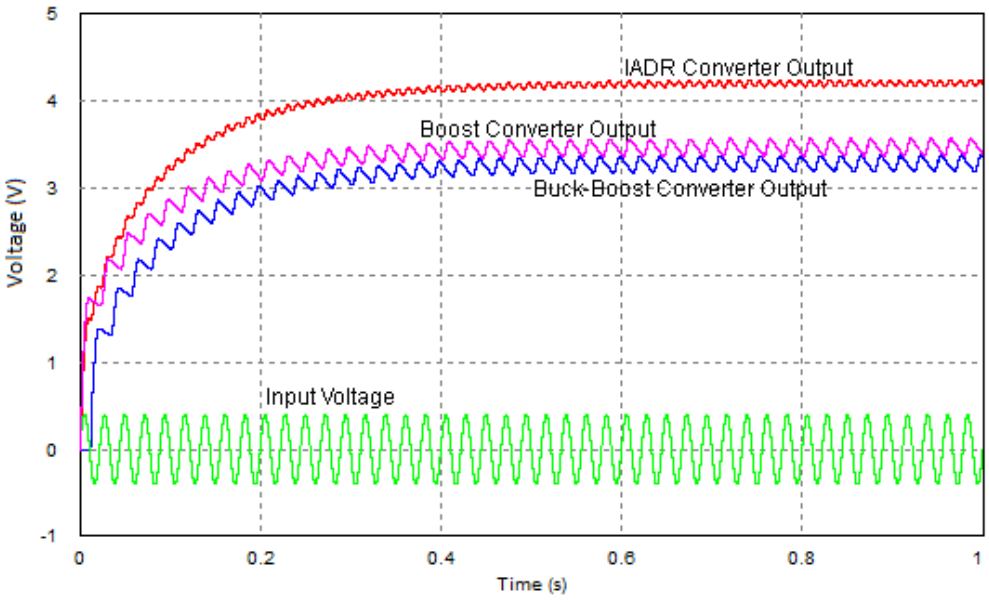

Fig. 3.10. Output voltage profiles for the different converters

The different output voltage profiles for the IADR converter (in red), the boost converter (in purple), and buck-boost converter (in blue) are shown in Figure 3.10. The corresponding input voltage is also shown in the same figure (in green). As the converters start operating, they start building the output voltage level in small steps until they reach a steady state where the voltage level stabilizes. As mentioned before, the boost converter is only operating during the positive input cycle and is seen to start delivering output voltage right from the beginning of the positive input cycle. The buck-boost converter is operating only during the negative half cycle and is seen to start delivering output voltage from the beginning of the first negative half cycle. Both these converters are seen to be able to step up the input voltage, however, for the same parameters and duty cycle, the IADR converter is seen to perform much better in terms of stepping up the input voltage. Also, since voltage is being stepped-up from both positive and negative cycles, the output voltage ripple is also very low for the IADR converter.

Some more results are presented in Figure 3.11. Figure 3.11 (a) shows the relationship of the output voltage varied with switching frequency, with duty cycle and load resistance kept fixed. As expected, increasing switching frequency results in decrease in output voltage converter due to increase in switching losses. Figure 3.11 (b) shows output voltage increasing with increase in load resistance in order to deliver the same power to the load.

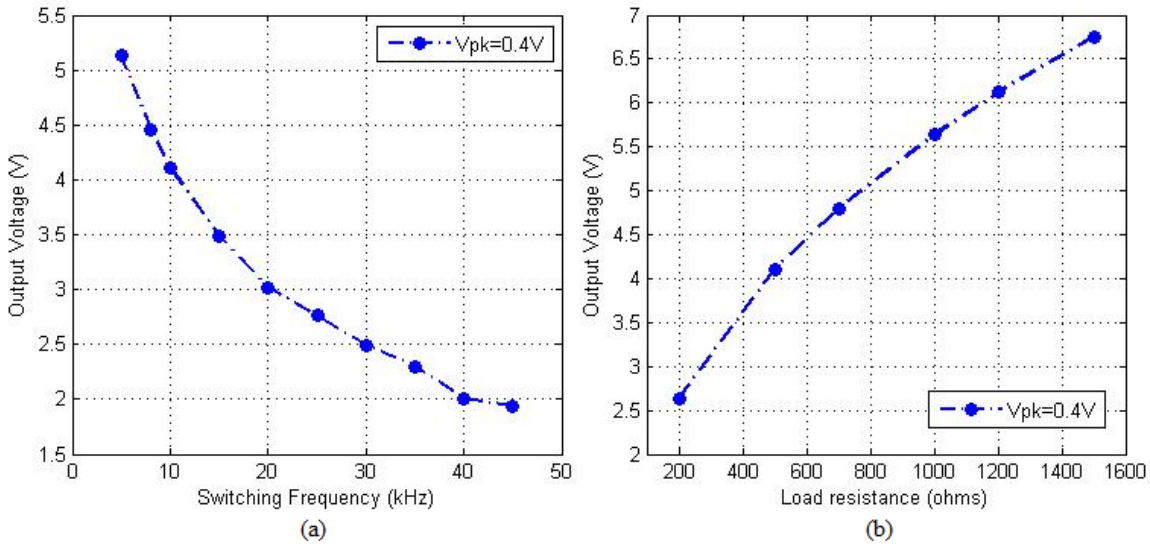

Fig. 3.11. (a) Output voltage and switching frequency relationship with fixed duty cycle and load (b) Output voltage and load resistance relationship with fixed duty cycle and switching frequency

Since the main objective of the IADR converter is to rectify and supply DC voltage to the load or battery from the piezoelectric transducer, it is important to check the voltage output levels for different output levels. In Section 2.5.1 it has been seen that the transducer is able to produce output voltage within the range of 300-600mV which acts as the input voltage to the IADR converter. Figure 3.12 shows the voltage output levels for input voltages with different amplitude levels. The output voltage increases almost linearly with increase in duty cycle when the switching frequency and load is kept constant.

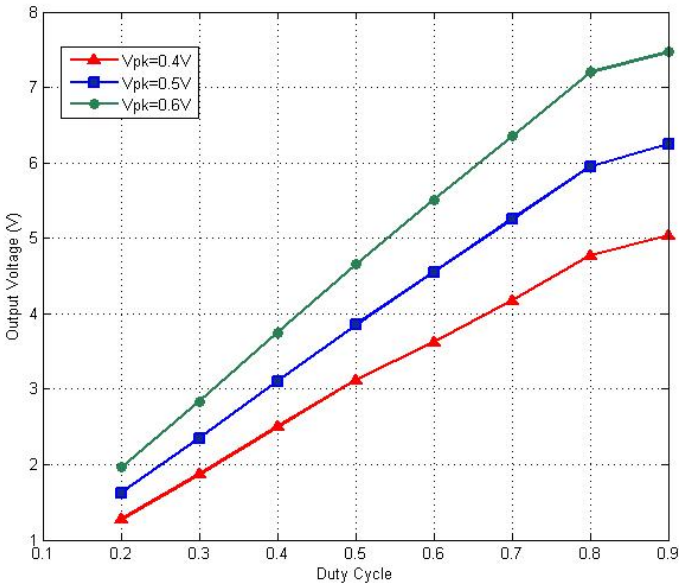

Fig. 3.12. Output voltage profiles for different input voltages

Hence it confirms that if the input AC voltage amplitude and other converter parameters are known, then the desired DC output voltage can be achieved by simply varying the duty cycle of the switches.

3.5.2. Closed Loop Simulation

From section 3.4 it has been confirmed that the IADR converter is able to successfully boost up and deliver a desirable DC output voltage to the load side. The desired output voltage level can be achieved by changing the duty cycle of the converter, given the input voltage amplitude is known. Since an objective of this study is to extend the application of the converter as a charger for a thin film Li-ion battery, special consideration should be given to ensure proper charging voltage is supplied by the converter. Commercially available thin film Li-ion cells can be charged by a constant recharging voltage of 4.1V under the constant-voltage charging scheme [41]. Voltage levels below the cell voltage will not charge the battery and voltage level higher than the charging voltage will be dangerous in such a charging scenario. Hence it is important to

include a controller that will boost up the AC voltage and keep it steady at the charging voltage level for all low amplitude input voltages.

3.5.2.1. Simulink implementation of PI controller

Since a constant amplitude impulse is applied to the piezo-film at a constant frequency, the input into the converter from the piezoelectric transducer is AC, the instantaneous value of the input voltage changes from zero to a maximum peak, goes back to zero and reaches a negative peak. Besides this there is no sudden change in the maximum amplitude level or frequency. Hence a simple proportional-integral, or PI controller can be easily implemented and is enough to regulate the output voltage to a nominal value of 4.1V.

Going back to the fact that the IADR converter is basically made of a boost and a buck-boost converter working in parallel, each with its own switch duty cycle, two individual PI controllers are used here to generate the duty cycles and gate pulses separately for each switch. The Simulink implementation of the PI controller for the boost converter is shown in Figure 3.13.

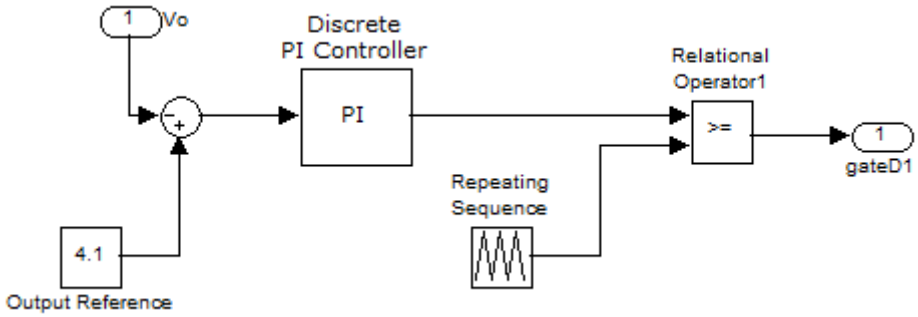

Fig. 3.13. Simulink implementation of PI controller

The input port V_o brings the actual output voltage of the converter. The constant block is used to set the desired output voltage reference. The error difference between the actual and the reference value is calculated and the difference is fed into the discrete PI controller block. The PI block has two parameters, the proportional gain (*Kp*) and the integral gain (*Ki*). The proportional gain was set to 0.001 and the integral gain was set to 0.6. The output from the PI controller block is the duty cycle generated for the corresponding switch.

A repeating sequence block is used to set the frequency of the gating pulses. The output from the PI controller and the repeating sequence block is compared using a relational operator to generate a pulse-width modulation (PWM) and the gating pulses are generated appropriately. A second PI controller with similar parameters is made for the buck-boost converter to generate the duty cycle and gating pulses of the buck-boost converter switch. The two controllers work together to keep the output voltage steady at the desired output level.

The output voltage from the IADR converter when both the controllers are operating is shown in Figure 3.14. Figure 3.14 (a) shows the output voltage when the output after reaching a steady state for an AC input voltage of maximum amplitude of 400mV. A closer look into the output in Figure 3.14 (b) shows how the output voltage (in red) is following the reference voltage (in blue) of 4.1V. The output voltage ripple is between $\pm$50mV. The corresponding steady state duty cycles for switches S1 and S2 generated by the PI controller are shown in Figure 3.15.

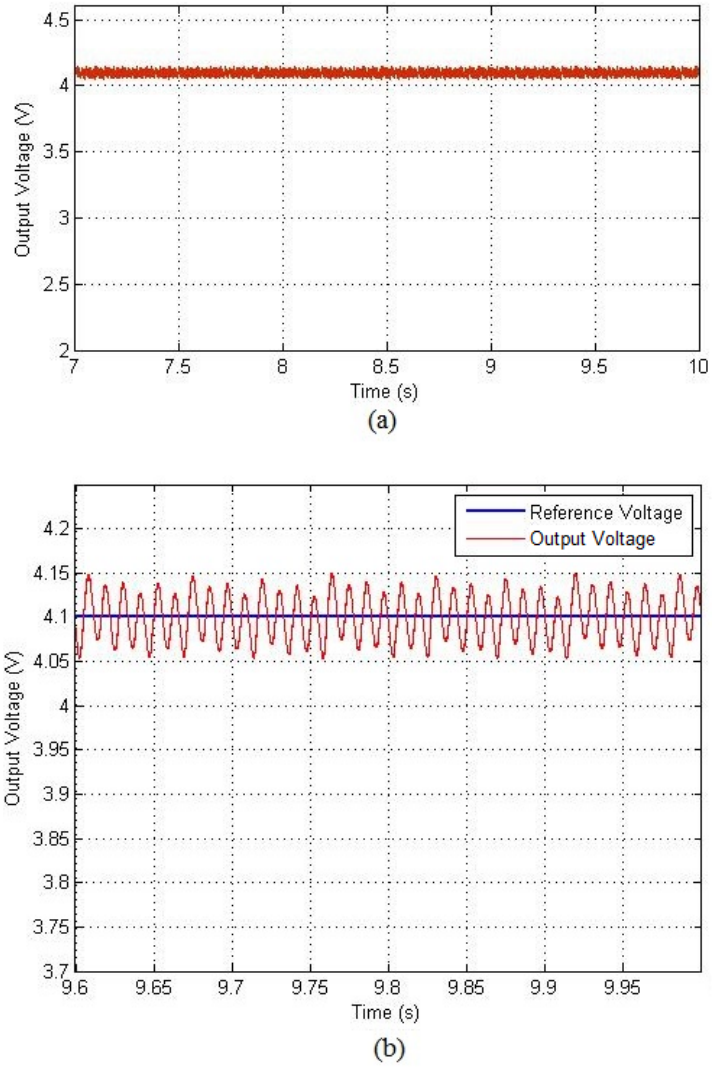

Fig. 3.14. (a) Closed loop output voltage (b) Output voltage and reference voltage

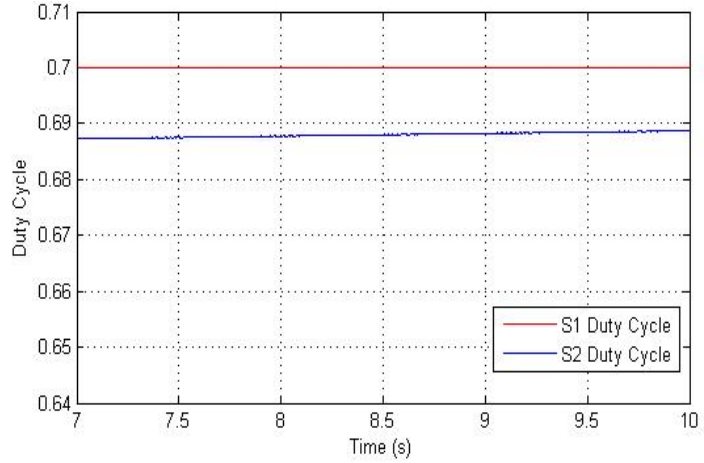

Fig. 3.15. Duty cycles of switches S1 and S2

The output voltage is always regulated at 4.1V. Therefore for a load of 500Ω, the output power is about 34mW. The performance of the converter under different input and load conditions are presented in Figure 3.16 and Figure 3.17. Figure 3.16 shows how the efficiency is varying with change in input voltages for particular load conditions. The relationship between the converter efficiency and load resistance for particular voltage inputs is shown in Figure 3.17.

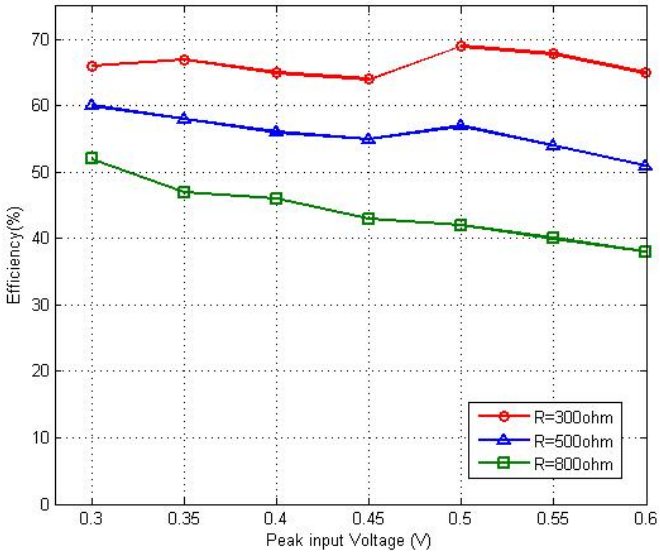

Fig. 3.16. Efficiency with variation of input voltage

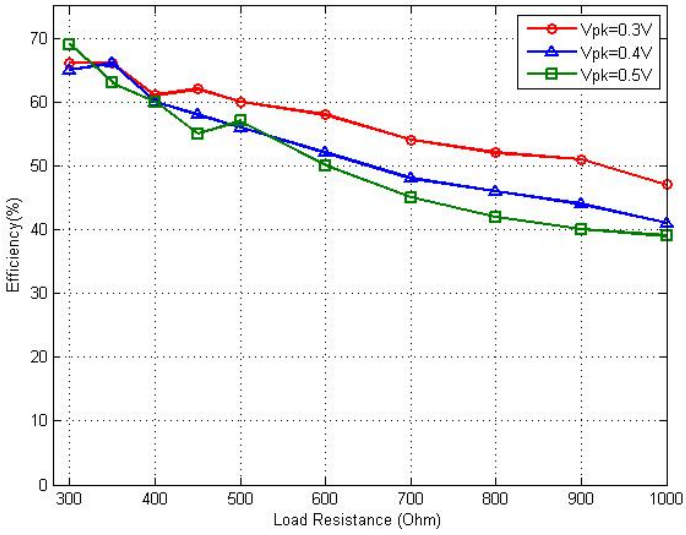

Fig. 3.17. Efficiency with variation of load

3.5.3. Lithium-Ion Cell Charging Performance

After establishing that the IADR converter is able to generate the required charging voltage for battery cell recharging purpose, it is important to investigate the performance using a real battery model and parameters. Literature evaluates a few commonly used circuit models for Lithium-ion battery like the Rint model, the RC model, the PNGV model, the DP model [42], it is important to note that every battery model is suitable for a specific application. A resistor in parallel with a capacitor (or the RC model) is usually used to load test battery charging circuits, although not the most accurate model, it is the most widely used model. Under constant voltage charging scheme, the percentage state of charge (SoC) of the battery cell is a good indicator to investigate if charge is being stored into the cell [43].

MATLAB/Simulink provides its own battery model which can be used for the simulation purposes when connected to the converter load side. The model is shown in Figure 3.18 and gives accurate results in terms of SoC when battery parameters are stated. The parameters chosen for simulation purposes are from the commercially available Thinergy MEC202 thin-film Li-ion micro-energy cell [41] and shown in Table 3.2. The battery cell can be used in applications like energy harvesting solutions/self-powered systems. Any constant voltage (CV) charge greater than the cell voltage (provided not exceeding the maximum specified voltage) will result in safe and rapid charging. CV charging method like direct connection to a power supply (in this case, the rectified converter output) can be used for recharging and is fast and totally safe regardless of the state of charge of the battery cell. If the battery is getting charged properly then it should be evident from the increase in the SoC percentage from its initial value.

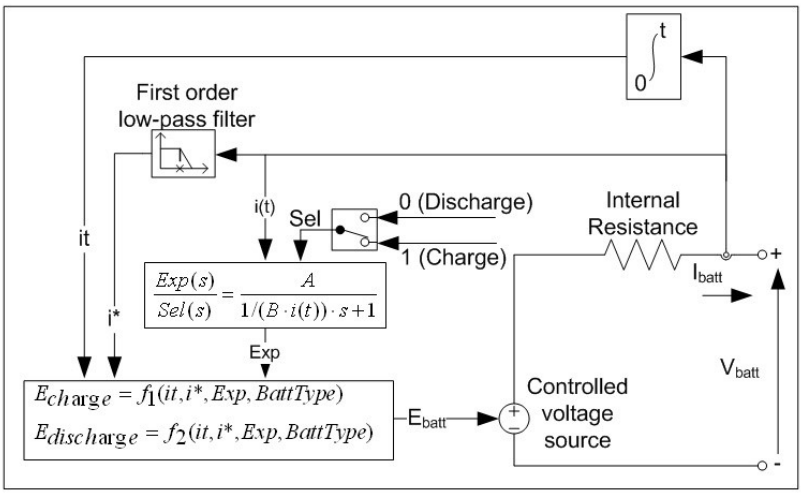

Fig. 3.18. Simulink Battery Model

Table 3.2. Lithium-Ion Cell Parameters

Nominal Voltage	3.9 V
Rated Capacity	2.2 mAh
Fully Charged Voltage	4.1 V
Nominal Discharge Current (A)	0.75 mA
Internal Resistance	22Ω
Recharge voltage	4.10 V Constant Voltage
Initial State of Charge (%)	50

When the Li-ion battery model is connected to the load side of the converter, as long as the output voltage of the converter is lower than the battery voltage, the battery night actually start discharging in the reverse direction instead of getting charged. This voltage is usually the battery nominal voltage. It should be noted that the IADR converter takes some time to boost up the input voltage into the desired charging voltage level. Therefore there is a fall in the SoC level initially during the charging process. This phenomenon is shown in Figure 3.19.

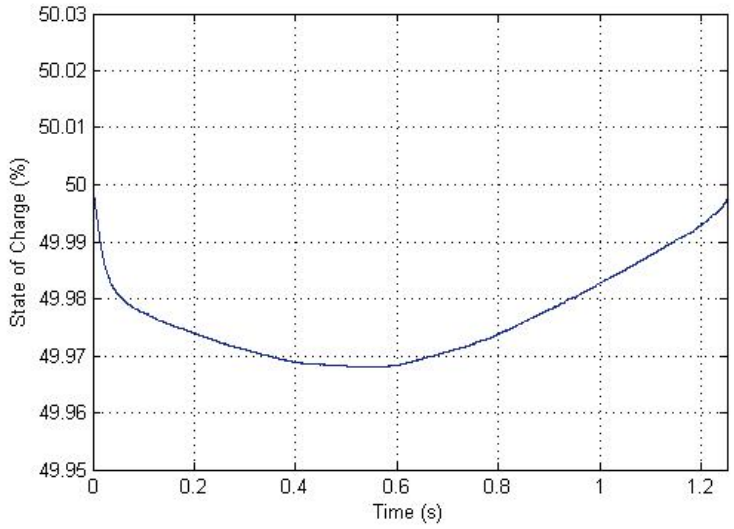

Fig. 3.19. Initial State of Charge of Li-ion Battery Cell

Figure 3.19 shows the state of charge level of the Li-ion battery cell when connected directly to the converter. This can be explained by the converter output voltage level as mentioned before. As long as the converter output voltage is lower than the battery nominal voltage, the SoC decreases as the battery starts discharging. As soon as the converter output level rises above the battery nominal voltage (at 0.7 seconds) the SoC level is seen to increase.

Although this effect is negligible and presents no drawback during the charging process (SoC drop is only about 0.04%), it can still be eliminated using a forward blocking diode. When a blocking diode is connected between the charging terminal of the converter and the battery, the battery cannot discharge as before and the SoC stays at the initial value until the converter output voltage surpasses the battery nominal voltage and the SoC level begins to increase (at around 0.7 seconds). The effect of the forward blocking diode on the SoC level is shown in Figure 3.20.

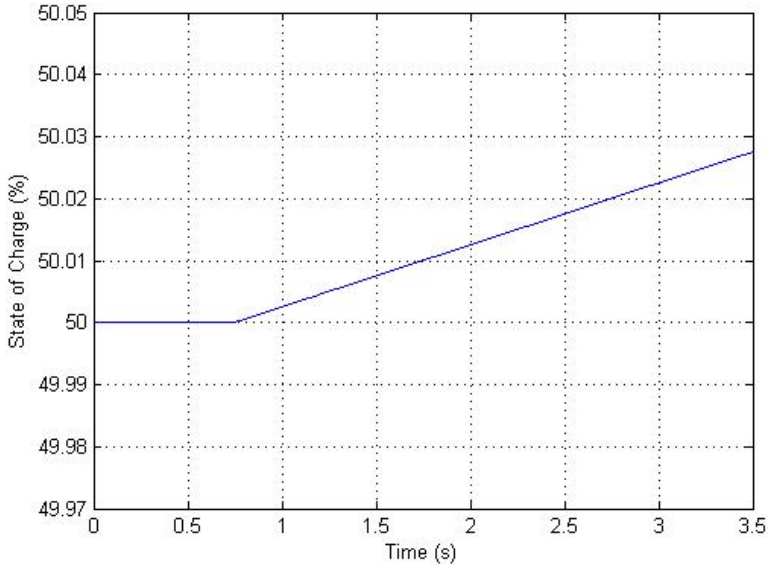

Fig. 3.20. SoC (%) of Li-ion Battery Cell with blocking diode

Figure 3.21 shows the state of charge percentage of the Li-ion battery cell charged by the IADR converter over a period of 150 seconds. The result shows a steady linear increase in the SoC level showing that the converter is performing successfully as a charger and storing charge into the cell using the constant voltage (CV) charging method.

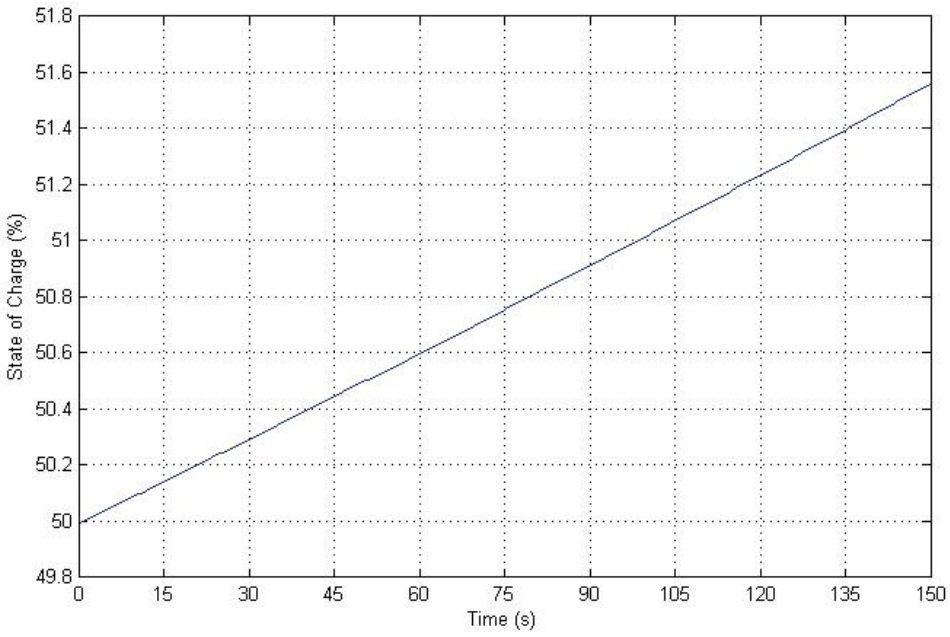

Fig. 3.21. SoC (%) of Li-Ion battery cell charged by IADR converter

3.6. Summary of Chapter 3

A single stage integrated AC-DC rectifier converter circuit is presented in this chapter that is able to rectify small AC input voltage and step it up into a more usable DC voltage without the use of a full bridge diode rectifying circuit. The stages of operation and the design principles of the converter is also discussed. The simulation results prove that the converter is applicable for energy harvesting applications with very low input voltage sources like from piezoelectric sources. The converter is also shown to be able to act as a charger and charge low power Li-ion thin film battery cells under constant voltage charging scheme.

Chapter 4.

EXPERIMENTAL SETUP AND POWER CONVERTER PROTOTYPE

4.1. Introduction

As mentioned earlier, a primary aim of this thesis is to build a power converter topology that is suitable for working with very low input voltage in the ranges of a few hundreds of millivolts. The previous chapter presented the basics of the IADR converter circuit and operational stages along with satisfactory simulation results. At this stage of the study, an experimental setup is intended to be assembled.

This chapter presents details of a laboratory prototype of the IADR converter and an open looped control implemented by a DSP interface to validate its performance in practical laboratory conditions. With experimental setup and test results, the theory explained previously can be validated.

4.2. Description of the Constructed Power Circuit

A power converter circuit was constructed in the laboratory from scratch using off-the shelf components to test the adopted IADR converter topology. This power circuit primarily contains six elements. First, is the buffered signal generator emulating the AC piezoelectric input to the converter. A power operational amplifier (Model LT1210CT7, Linear Technology) in voltage follower mode is used as the buffer circuit for the signal generator. The source amplitude and frequency could be easily set using the generator. Second are the ferrite core, copper wound, insulated inductors (Model B82111EC23, EPCOS) working as the energy harvesting elements. For switching applications, N-channel MOSFETs (Model STW70N60M2, STMicroelectronics) were chosen for both the boost and the buck-boost converter. The low on-state resistance and gate charge make

these switches ideal for the power circuit. Another crucial element for the circuit construction is the diode. Schottky diodes (RA13V1, Sanken) are chosen for their low forward threshold voltage drop of 0.3V compared to traditional silicon based diodes with drops of 0.7-0.8V. The last two elements are the smoothing capacitor (BC2665CT, Vishay) and a resistive load of 1kΩ. The values of these key converter components and parameters are presented in Table 4.1.

Table 4.1. Parameters of Converter Components

Source Amplitude	400 mV
Source Frequency	45 Hz
Switching Frequency	10 kHz
Boost Inductor	40 µH
Buck-Boost Inductor	40 µH
Output Capacitor	500 µF
Load Resistance	1000 Ω
Schottky Diode Forward Voltage Drop	0.3 V
MOSFET R_{ds} on	40 mΩ

Apart from the abovementioned components for the circuit, some other operational amplifier IC's like switch gate drivers and a zero-crossing detector were also implemented whose functions will be discussed later. Figure 4.1 shows a photograph of the constructed integrated AC-DC rectifier converter (IADR) circuit and its two constituent DC-DC boost and buck-boost converters.

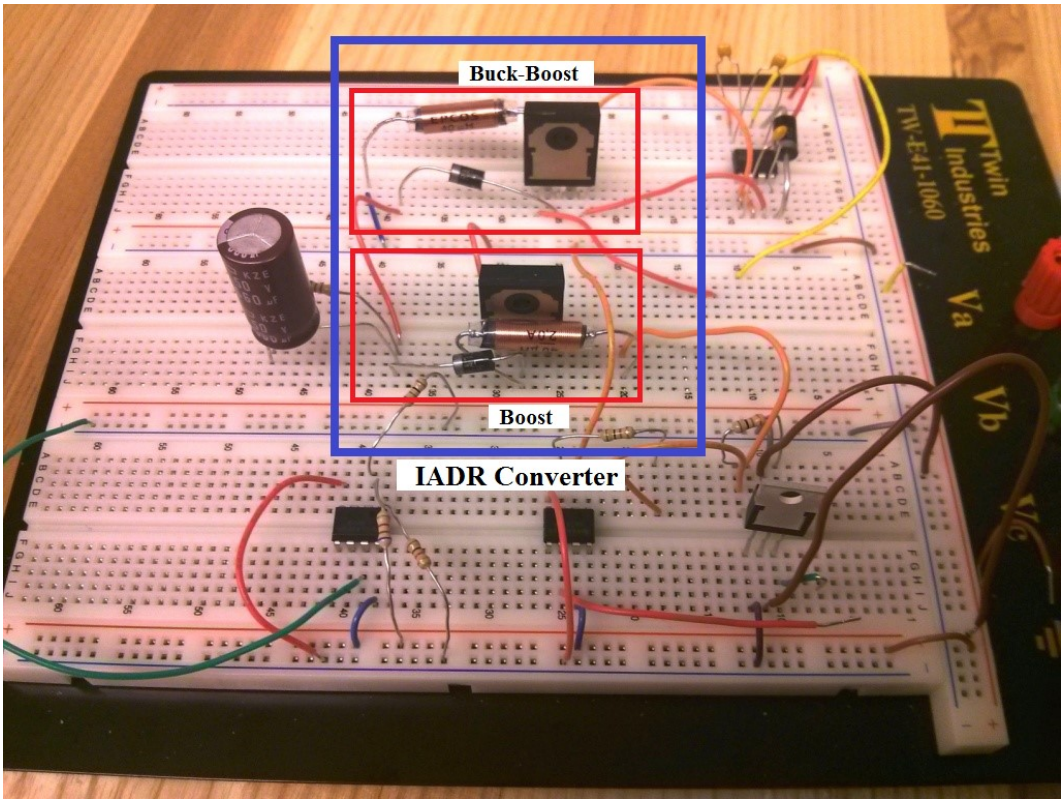

Fig. 4.1. Experimental prototype of the IADR converter circuit

4.3. Pulse Generator using dSPACE Development System

As it was discussed before in Chapter 3 (Refer to Section 3.3), the functioning of the IADR converter is dependent on the proper control over the switching scheme of the two switches. Typically in converters implementing two switches, e.g. synchronous converters, the switches operate in a complimentary fashion. But for the IADR converter, each switch operates at the switching frequency only for one half of the input cycle and remains completely turned off during the other cycle while the other one is switching. Therefore it is essential to design a pulse generator that meets the characteristics of this switch control strategy. A digital signal processor (DSP) development kit (DS-1103, dSPACE) was employed to monitor and implement this switching scheme of the converter.

4.3.1. DS-1103 Real-Time Interface to SIMULINK

The dSPACE system is a common hardware architecture that can be used for prototyping and controlling of electrical systems. It consists of a DS-1103 PPC controller board, a vast range of I/O devices are available on board and real-time interfacing permits running MATLAB/SIMULINK models on the controller board. The DS-1103 real-time interface enhances the SIMULINK block library by providing convenient configuration items like A/D converter, D/A converter, digital I/O and PWM signal generation. Utilizing the extended block library, a SIMULINK model can be built that has an effective control over the switching characteristics. Figure 4.2 presents the master PPC library found in the processor dSPACE DS-1103.

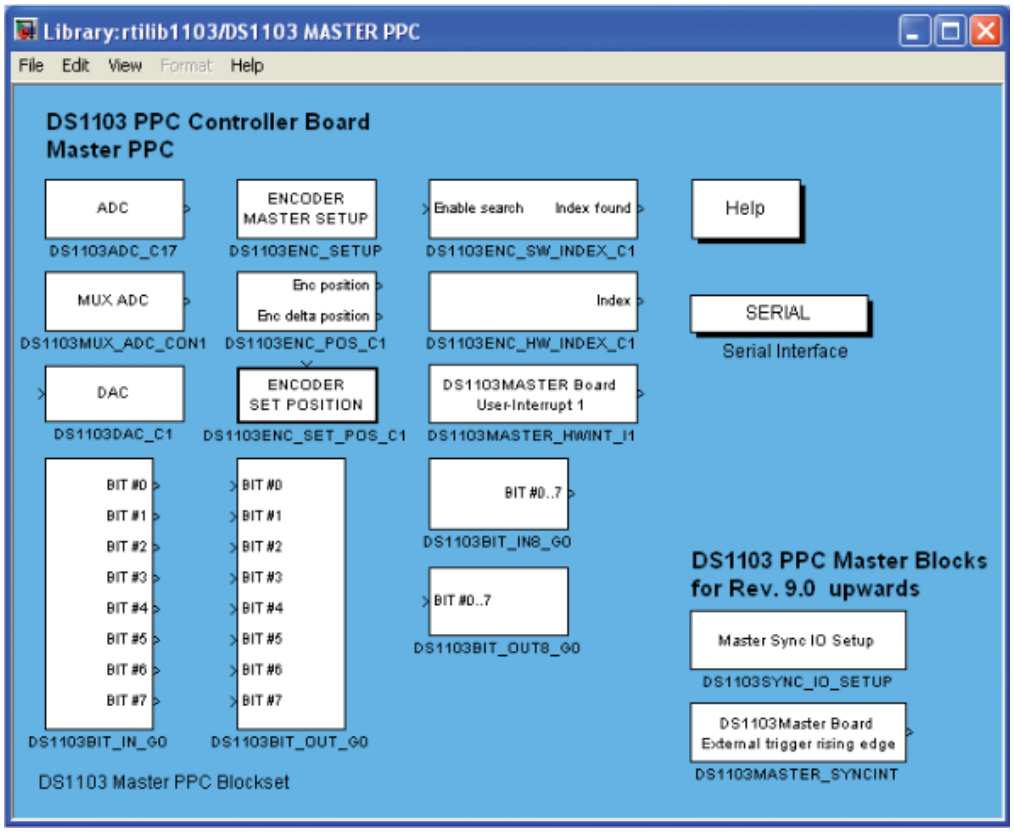

Fig. 4.2. DS-1103 real-time interface block library

Figure 4.3 presents the SIMULINK circuit diagram implemented for the experimental gate pulse generation for the MOSFET switches. The ADC (analog to digital conversion) block (DS1103ADC_C17) is used to bring the external signal into SIMULINK. The output of the signal generator is connected to the dSPACE ADC input. Proper gain adjustments is done using the Gain block because of the sensor and dSPACE gains. Relational operators are used to determine the positive and negative cycles of the input signal. The PWM block (DS1103SL_DSP_PWM) from the dSPACE library is used to generate the PWM gate pulses. Channel 1 and Channel 2 of the PWM block is used for the two individual switches and the remaining two channels are grounded. The constant blocks D1 and D2 are the duty cycles of the two switches.

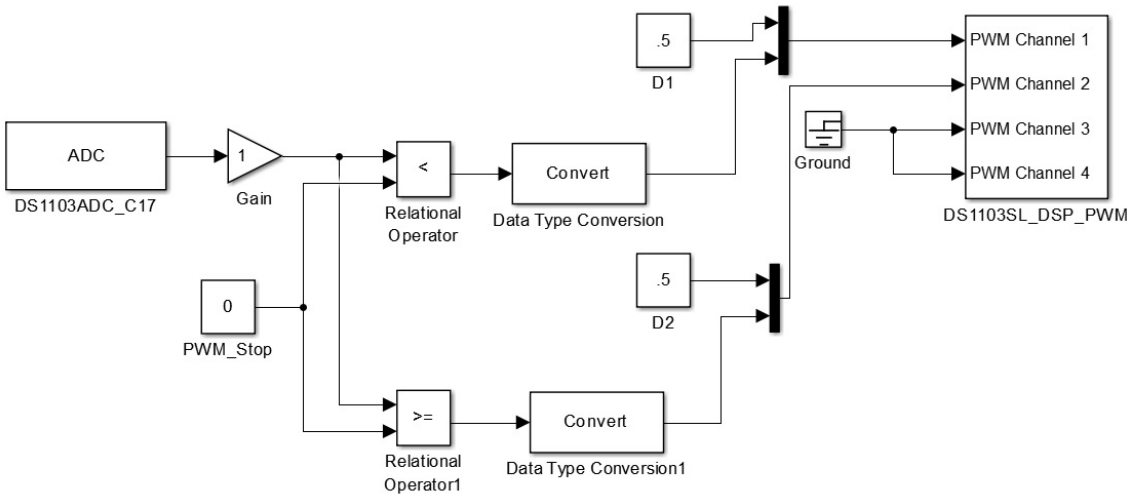

Fig. 4.3. SIMULINK implementation of the switch gate pulses for the experimental setup.

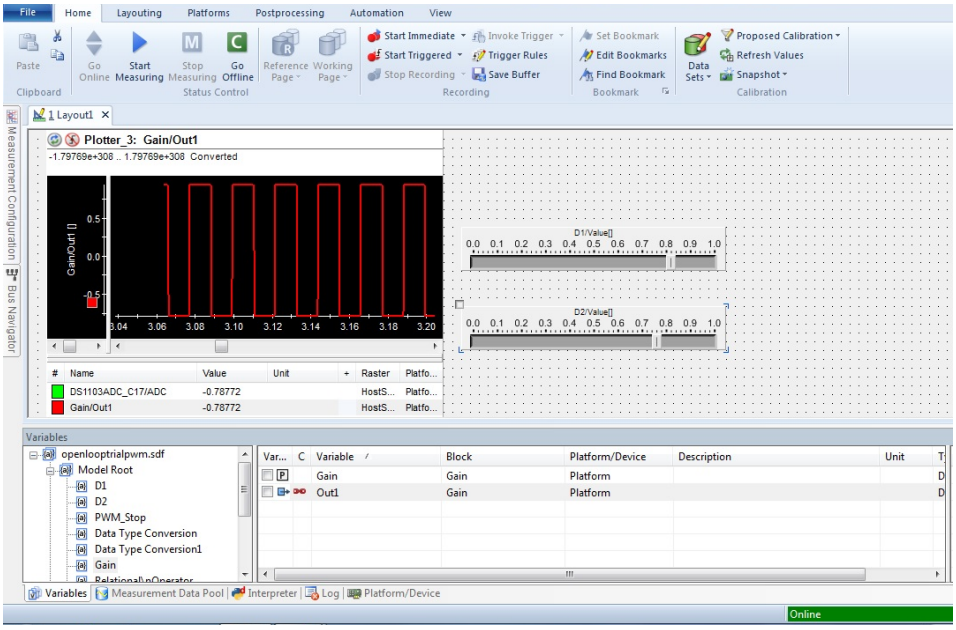

Fig. 4.4. Customize user friendly ControlDesk interface in dSPACE

The dSPACE ControlDesk is a user friendly interface for the DS-1103 dSPACE board. From the ControlDesk, experiment prototypes can be controlled, monitored and automated. A ControlDesk interface display was also created which would allow control over the switching parameters in real-time as shown in Figure 4.4. From the figure we can see the slide bars for controlling the duty cycles of the two switches.

4.4. Zero Crossing Detector and Gate Drivers

It is imperative that the gating voltages of the two converter switches are synchronized with the generator input voltage. Therefore the dSPACE controller must be able to detect a change in the input polarity for appropriate switching timing. This can be achieved by implementing a Zero-Crossing detector circuit which is generally used to generate a synced pulse that is related to the AC voltage phase. The circuit used for this purpose is the LM311, Texas Instruments comparator IC. The IC effectively detects the momentary zero value of the AC voltage and the signal is sent to the dSPACE controller

which then determines if the voltage polarity is positive or negative and sends gating pulses to the appropriate switch.

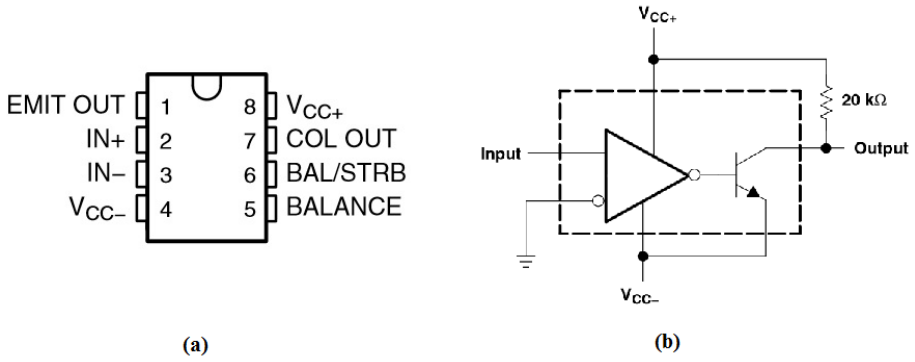

Fig. 4.5. (a) LM311 IC Schematic diagram (b) LM311 Zero Crossing Detector Circuit [44]

The gating signals generated by the dSPACE system usually presents low voltage (0-5V) and needs to be amplified (to 0-15V) to drive typical MOSFETs. Gate driver circuits are commonly used for driving such IGBT and MOSFET switches. However, a challenge was faced while using such MOSFET drivers for the IADR converter. The gate driver circuit ICs come with a ground pin which needs to grounded. This gave rise to the two MOSFETs and the signal generator having a common ground point which subsequently resulted in the generator input to the converter to get corrupted. The solution was to isolate the ground node of the generator and converter from the ground node of the gate driver circuits. The issue was addressed by implementing opto-isolated gate driver circuits (VO3120, Vishay Semiconductors) which separated the common ground nodes and provided the necessary amplified driving voltage to the MOSFET gate nodes. Bench power supply (EX355R, Thurlby Thandar Instruments) was used as power sources for driving the zero-crossing detector and gate driver circuit ICs.

4.5. Description of Experimental Test Bench

Figure 4.6 depicts the layout of the experimental test bench setup. The buffered signal generator emulates the piezoelectric transducer and the converter voltage input source. It is also connected to the Zero-crossing detector and the dSPACE DS-1103 controller board to track the positive and negative input cycles from the generator. The controllable parameters like the duty cycle of the MOSFETs are controlled in real-time using the dSPACE ControlDesk. The gating signals are processed and sent to the gate drivers by dSPACE which finally drives the MOSFET switches S_1 and S_2. A photograph of the experimental test bench built in the laboratory is shown in Figure 4.7.

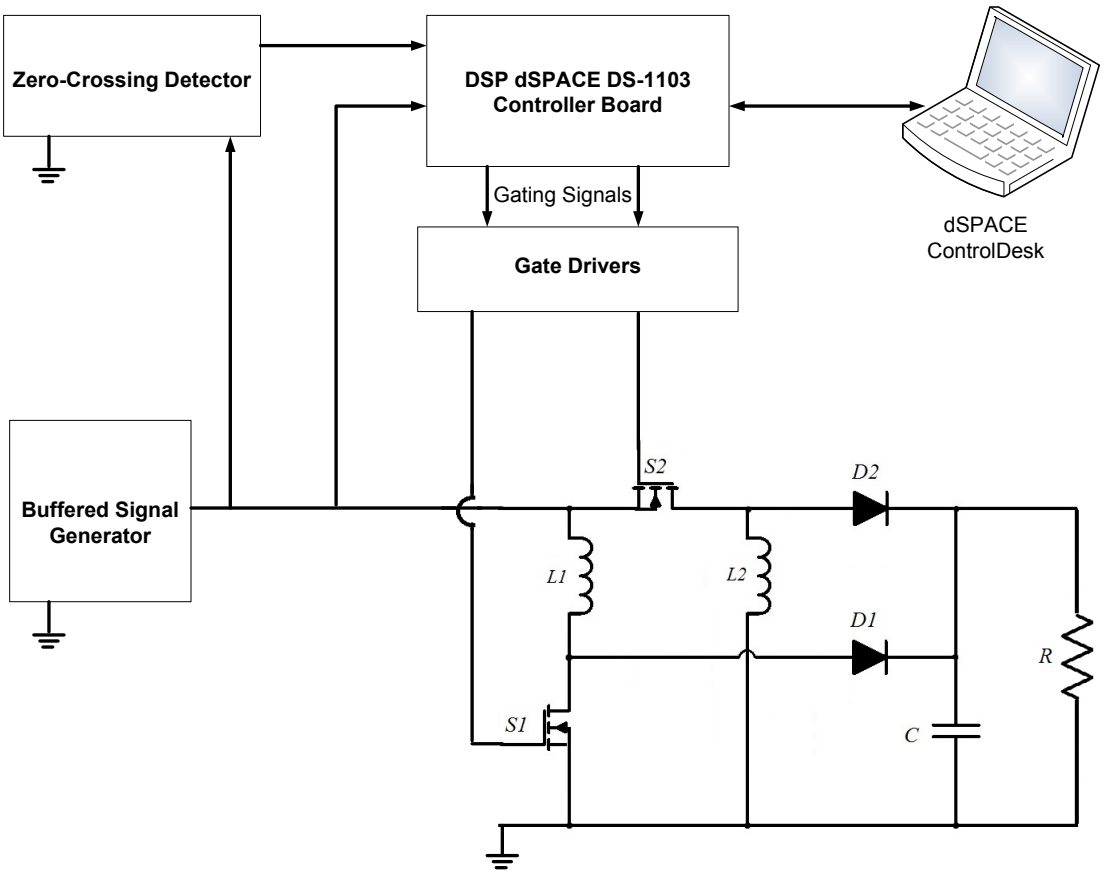

Fig. 4.6. Experimental setup diagram

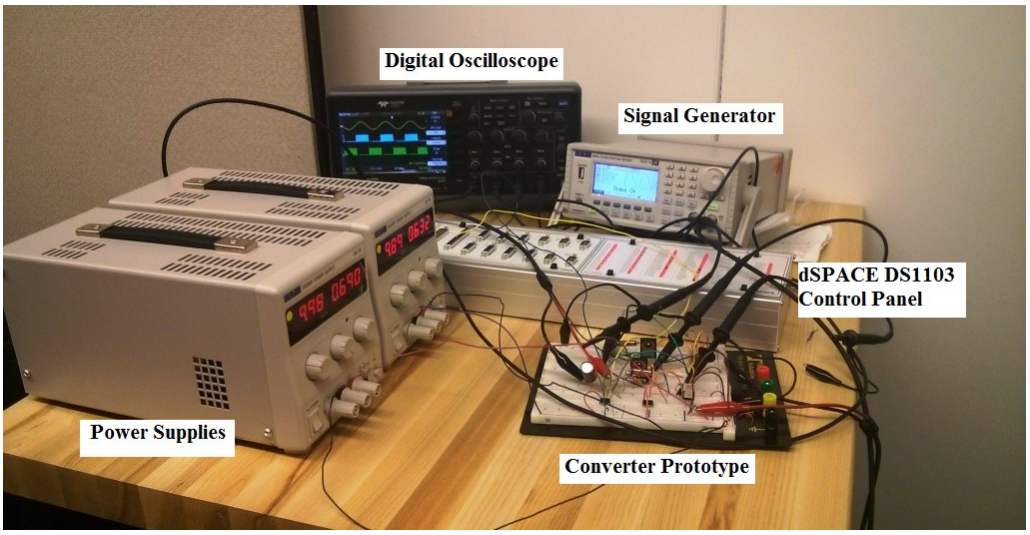

Fig. 4.7. Experimental test bench setup

4.6. Experimental Results

After setting up the experimental test bench, the IADR converter was run and data was collected to verify both the switching scheme of the converter and the converter's performance in rectifying the AC input signal. The signal generator is used to emulate the piezoelectric transducer under vibration and is set to supply an AC voltage signal of 400mV peak at a frequency of 45Hz which was determined to be the piezoelectric transducers resonant frequency in Chapter 2 (refer to section 2.5.1). The switching scheme implemented by the dSPACE system should now be able to detect the change in voltage polarity of the input signal with the aid of the zero-crossing detector and synchronize to switch MOSFET S_1 of the boost part of the converter during the positive cycle and MOSFET S_2 of the buck-boost converter during the negative cycle. Duty cycle for both the switches are set to 0.7 and the switching frequency is set to 10 KHz.

The MOSFETs S_1 and S_2's gate drive pulses supplied by the dSPACE is presented in Figure 4.8. The two gating pulses are perfectly synchronized with the converter input voltage (in blue). The boost converter's switch S_1 (in red) is seen to be operating only during the positive cycle and the buck-boost converter's switch S_2 (in green) is operating only during the negative cycle of the input. Figure 4.9 presents a closer look at the gating pulses at a zero-crossing moment and shows how the converter stops switching S1 and starts switching S2 as the input changes from positive to negative.

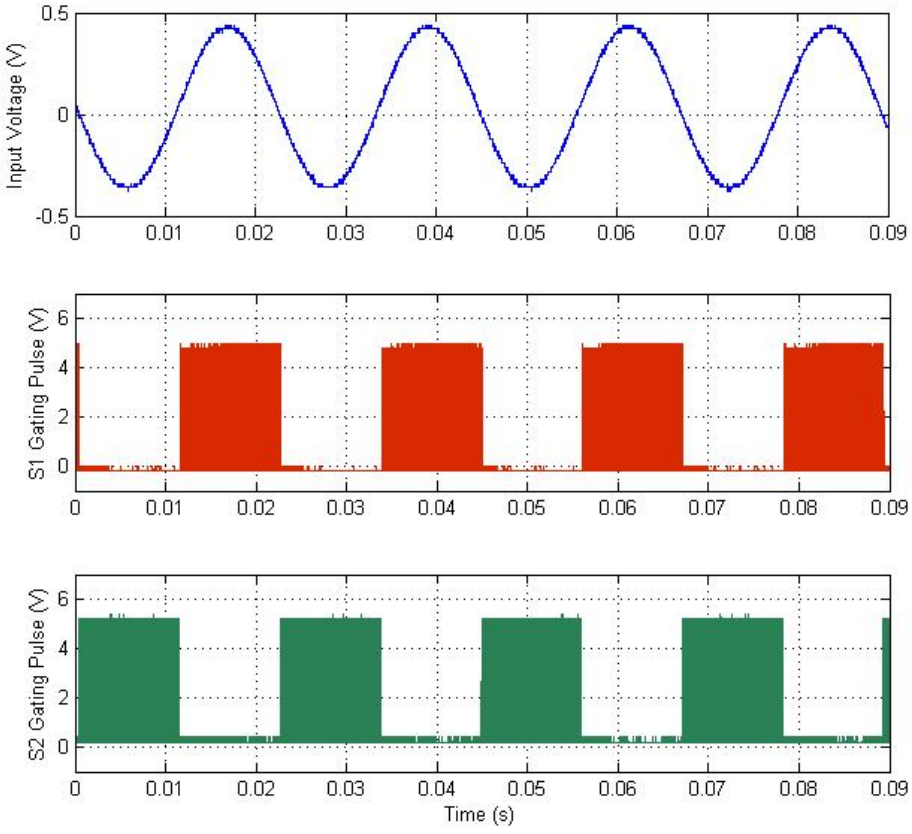

Fig. 4.8. Switches S1 and S2 gating pulses in relation with the converter input voltage

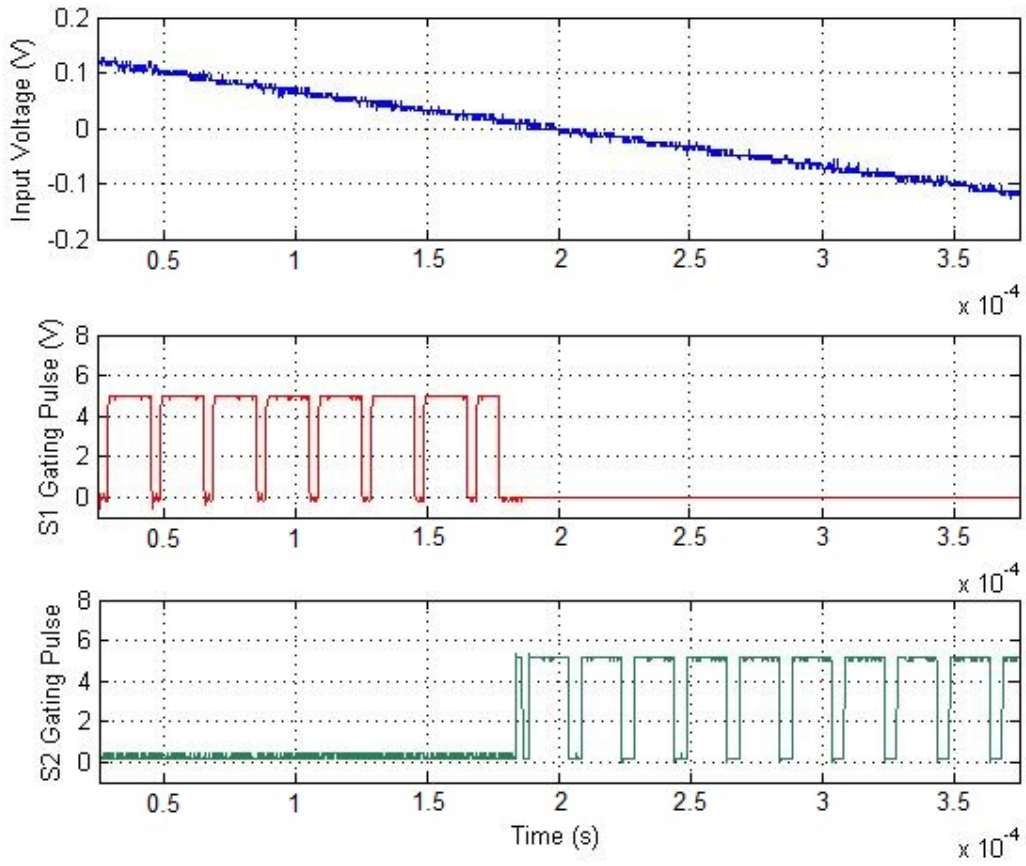

Fig. 4.9. Switches S1 and S2 gating pulses in relation with the converter input voltage at a zero-crossing scenario

The output voltage of the converter prototype is shown in Figure 4.10 (in red) in relation with the converter input voltage (in blue). It is seen that the low 400mV amplitude AC input voltage of about is successfully stepped-up to a much higher rectified DC value of about 3.7V. The rectified voltage is also seen to have very little ripple. This experimental result validates the concept of the integrated AC-DC rectifier converter presented in Chapter 3 that two individual DC-DC converters could be integrated into one to be used for each half cycle of the AC input respectively and obtain a boosted DC voltage.

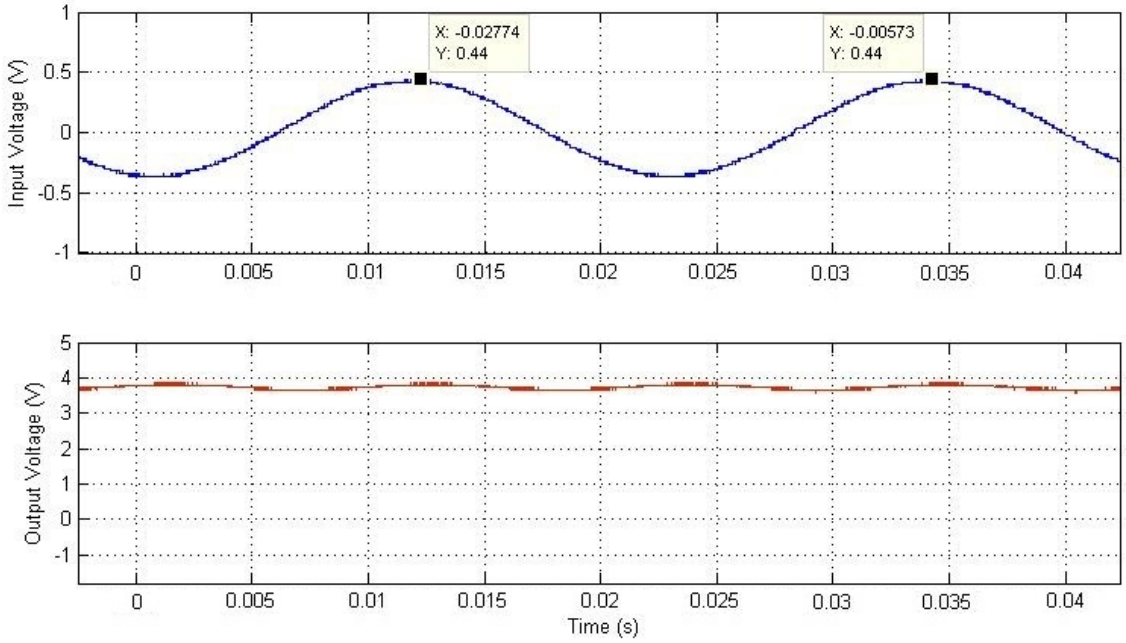

Fig. 4.10. Converter AC input voltage and rectified DC output voltage

Further test is conducted on the converter prototype by varying the duty cycles of the two switches. The result of the open looped converter performance is presented in Figure 4.11. The converter is able to rectify the low input voltage and boost it up successfully as predicted.

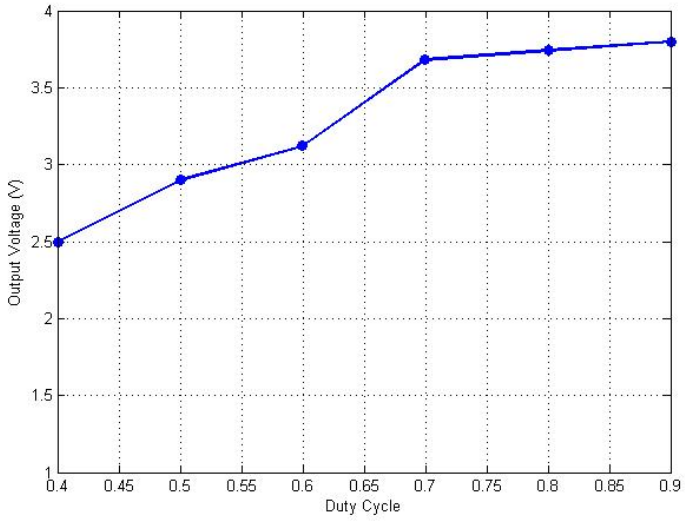

Fig. 4.11. Open loop plot of converter output voltage against switch duty cycle

Although an increase in duty cycle value resulted in an increase in the output voltage level, the voltage levels for each duty cycle is seen to be lower than expected. The voltage level is seen to get saturated at duty cycle of 0.7. Maximum output voltage level of 3.8V occurs at duty cycle 0.9. However, this behavior can be explained as to be the effect of the converter component parasitics. Inductor parasitics and switching losses will naturally be higher in practical scenarios than in simulation environment. Also, it should be noted that the prototype was assembled on a solderless breadboard, which presents a small amount of stray inductance. Typically it does not have an observable impact on circuits operations, but for such low input voltage as considered in this study, the effect is significant.

4.7. Summary of Chapter 4

This chapter includes the synthesis of the constructed power circuit, which is used to test the concept of the integrated AC-DC rectifier converter. It includes a description of the various incorporated elements that forms the experimental test bench. A pulse generator for switching scheme was implemented using the dSPACE system. Using the switching scheme, experimental results showed the converter to successfully be able to rectify and boost millivolts range of AC voltage into a usable DC voltage with minimum ripple. Controllable parameter like the switch duty cycle and its effect have been discussed and experimental results were presented depicting practical scenario.

Chapter 5.

CONCLUSION OF THESIS

5.1. Summary of Thesis

The main focus of this M.A.Sc. thesis was on piezoelectric micro-energy harvesting and designing a power converter for low-input voltage resulting from weak vibrations. Vibration is ubiquitous in the environment surrounding us and is considered as one of the major sources of micro-energy harvesting. The main advantage that piezoelectric energy harvesting provides is that it captures energy that would otherwise have been wasted. An efficient energy harvesting system design requires examination of both the transducer and the harvesting converter, for a particular end system application. Besides supplying power to small loads, battery charging from ambient vibration source is another end application worth researching on.

An overview of energy harvesting and piezoelectric theory is presented in Chapter 1. It also presents a brief survey of the commonly used power converter topologies for piezoelectric energy harvesting, showing that most of these converters are based on full bridge diode rectifier circuit followed by a DC-DC converter. It becomes evident that this two-stage rectifying process is not suitable for interfacing with transducers that produce extremely low voltage as it would be lost in the very first stage overcoming the diode rectification process.

Chapter 2 presented the details of a piezoelectric mechanical transducer. A small Polyvinylidene Fluoride (PVDF) based piezoelectric thin film was studied and its characteristics as a transducer was investigated. The derivation of the transducer's electrical equivalent circuit as a voltage source was discussed displaying the transducer's electrical response as an AC voltage source under a constant periodic vibration. An

experimental vibration setup was also built to test the transducer under impulse-based vibration using a vibrational shaker. Measurements done with the transducer is of special importance in order to determine the range of output voltage from the transducer that the power converter would expect as input. Experimental results showed the range of output voltage amplitude to be within 300-600mV. The experimental study also revealed the resonant frequency of the transducer to be about 45Hz with which the power converter switching scheme must be synchronized.

The proposed single-stage integrated AC-DC rectifier converter was investigated in details in Chapter 3. The converter topology effectively eliminated the use of a full bridge diode rectifier by integrating two separate DC-DC converters for each cycle of the AC input voltage. Also, conventional diodes in the converter were replaced by Schottky diodes with lower threshold voltage. As a result, additional voltage losses across the rectifier is avoided and the converter significantly reduces the threshold voltage level that the transducer had to produce for effective harvesting. The different stages of converter operation and design principles are also analyzed. Simulation results confirmed that the converter is able to rectify and boost input voltages in the range of few hundred millivolts to a stable, more usable DC voltage under open loop conditions, and with a step-up ratio over 10. A simple proportional integral controller was also implemented to assess the converter's ability to regulate the output at a nominal DC voltage value of 4.1V, and decent efficiency levels from 50-70% were achieved under varying input voltage and varying load conditions. The inclusion of an energy storage element as an end application system was also done to check the converter's performance in battery charging applications. Thin film lithium-ion cell was chosen because of its high energy density and growing popularity as energy storage element from energy harvesting applications. A MATLAB/SIMULINK battery model was implemented with commercial Li-ion cell

parameters at the load side of the converter. The converter supplied a steady charging voltage of 4.1V and the subsequent steady increase in the cell's state of charge established the converter's versatility to be used as a battery charger under constant-voltage charging scheme.

Finally, Chapter 4 includes the open loop experimental assessment of the IADR converter concept. A description of the experimental setup, the constructed power converter circuit and employed apparatus were also presented in this chapter. The DSP development kit dSPACE DS-1103 was employed to implement the switching scheme, along with a user friendly interface which allowed variation and monitoring of the controllable parameters. A DC output voltage of 3.8V was harvested from a nominal AC input voltage of 400mV amplitude showing that the converter is able to supply a stable DC voltage which can also be used for powering a small load or cell charging applications.

5.2. Suggestions for Future Work

Over the course of this research, some important opportunities were found which could direct towards the continuity of this work, and investigation of which would enhance this study and add value to the research. Some suggestions for future work are;

- Conduct transducer experiments with quantified vibration levels to develop a simulation model for predicting the piezoelectric transducer output nature.
- Evaluate the converter performance by eliminating all diodes and incorporating switches instead to employ synchronous rectification.
- Develop a controller to operate the converter at a wideband input frequency range. The controller could provide robustness by being stand-alone and able to operate when external power source cannot be assured.

- Calculate and analyze MOSFET and diode switching losses to develop a realistic efficiency profile.
- Constructing and evaluating the converter circuit on a printed circuit board to remove the effects of stray inductances, conduction losses and device parasitics.

BIBLIOGRAPHY

[1] J. Carrasco, L. Franquelo, J. Bialasiewicz, E. Galvan, R. Guisado, M. Prats, J. Leon and N. Moreno-Alfonso, "Power-Electronic Systems for the Grid Integration of Renewable Energy Sources: A Survey," *IEEE Transactions on Industrial Electronics,* vol. 53, no. 4, pp. 1002-1016, 2006.

[2] F. Yildiz, "Potential Ambient Energy-Harvesting Sources and Techniques," *The Journal of Technology Studies,* vol. 35, no. 1, pp. 40-48, 2009.

[3] V. Raghunathan, A. Kansal, J. Hsu, J. Friedman and M. Srivastava, "Design Considerations for Solar Energy Harvesting WIreless Embedded Systems," *Fourth IEEE/ACM International Conference on Information Processing in Sensor Networks,* 2005.

[4] E. Dawidowicz, "Wind Energy Harvesting for Low Power Applications," *SAE International Journal of Aerospace,* vol. 1, no. 1, pp. 883-886, 2009.

[5] R. Ang, Y. Tan and S. Panda, "Energy Harvesting for Autonomous Wind Sensor in Remote Area," *33rd Annual Conference of IEEE Industrial Electronics Society,* pp. 2104-2109, 2007.

[6] E. Carlson, K. Strunz and B. Otis, "A 20mV Input Boost Converter with Efficient Digital Control for Thermoelectric Energy Harvesting," *IEEE Journal of Solid-State Circuits,* vol. 45, no. 4, pp. 741-750, 2010.

[7] M. Koplow, A. Chen, D. Steingart, P. Wright and J. Evans, "Thick Film Thermoelectric Energy Harvesting Systems for Biomedical Applications," *IEEE 5th International Summer School and Symposium on Medical Devices and Biosensors,* pp. 322-325, 2008.

[8] A. Erturk and D. Inman, Piezoelectric Energy Harvesting, Wiley, 2011.

[9] "IEEE Standard on Piezoelectricity," in *Standards Commitee of the IEEE Ultrasonics, Ferroelectrics, and Frequency Control Society*, New York, Institute of Electrical and Electronics Engineers, 1987.

[10] K. Uchino, "Ferroelectric Devices," New York, Marcel Dekker Inc., 2000.

[11] J. Nye, "Physical Properties of Crystals," Oxford: Oxford University Press, 1957.

[12] D. Scansen, "Understanding Storage Battery Specifications for Energy Harvesting," Digi-Key Corporation, 21 Sep 2011. [Online]. Available: http://www.digikey.com/en/articles/techzone/2011/sep/understanding-storage-battery-specifications-for-energy-harvesting. [Accessed Jan 2015].

[13] D. Scansen, "Storage Battery Solutions for Energy Harvesting Applications," Digi-Key Corporation, 18 July 2012. [Online]. Available: http://www.digikey.com/en/articles/techzone/2012/jul/storage-battery-solutions-for-energy-harvesting-applications. [Accessed Aug 2014].

[14] A. Shafiei, "Modeling, Analysis and Design of a PV-Based Grid-Tied Plug-in Hybrid Electric Vehicle Battery Pack Charger," Concordia University, Montreal, 2013.

[15] G. Ottoman, H. Hoffmann, A. Bhatt and G. Lesieutre, "Adaptive Piezoelectric Energy Harvesting Circuit for Wireless Remote Power Supply," *IEEE Transactions on Power Electronics,* vol. 17, pp. 669-676, 2002.

[16] G. K. Ottman, H. F. Hofmann and G. A. Lesieutre, "Optimized Piezoelectric Energy Harvesting Circuit Using Step-Down Converter in Discontinuous Conduction Mode," *IEEE Transactions on Power Electronics,* vol. 18, no. 2, pp. 696-703, 2003.

[17] M. Guan and W. Liao, "On the Efficiencies of Piezoelectric Energy Harvesting Circuits Towards Storage Device Voltages," *Smart Materials and Structures,* vol. 16, pp. 498-505, 2007.

[18] M. Guan and W. Liao, "Characteristics of Energy Storage Devices in Piezoelectric Energy Harvesting Systems," *Journal of Intelligent Material Systems and Structures,* vol. 19, pp. 671-679, 2008.

[19] E. Lefeuvre, D. Audigier, C. Richard and D. Guyomar, "Buck-boost Converter for Sensorless Power Optimization of Piezoelectric Energy Harvester," *IEEE Transactions on Power Electronics,* vol. 22, pp. 2018-2025, 2007.

[20] N. Kong, D. Ha, A. Erturk and D. Inman, "Resistive Impedance Matching Circuit for Piezoelectric Energy Harvesting," *Journal of Intelligent Material Systems and Structures,* vol. 21, 2010.

[21] D. Guyomar, A. Badel, E. Lefeuvre and C. Richard, "Toward Energy Harvesting Using Active Materials and Conversion Improvement by Nonlinear Processing,"

IEEE Transactions of Ultrasonics, Ferroelectrics, and Frequency Control, vol. 52, pp. 584-595, 2005.

[22] A. Badel, A. Benayad, E. Lefeuvre, L. Lebrun, C. Richard and D. Guyomar, "Single Crystals and Nonlinear Process for Outstanding Vibration-Powered Electrical Generators," *IEEE Transactions on Ultrasonics, Ferroelectrics, and Frequency Control,* vol. 53, no. 4, pp. 673-684, 2006.

[23] Y. Ramadass and A. Chandrakasan, "An Efficient Piezoelectric Energy Harvesting Interface Circuit Using a Bias-flip Rectifier and Shared Inductor," *IEEE Journal of Solid-State Circuits,* vol. 45, no. 1, pp. 189-204, 2010.

[24] D. Kwon and G. Rincon-Mora, "A Rectifier-Free Piezoelectric Energy Harvester Circuit," *IEEE International Symposium on Circuits and Systems,* pp. 1085-1088, 2009.

[25] D. Kwon and G. A. Rincon-Mora, "A 2μm BiCMOS Rectifier-Free AC-DC Piezoelectric Energy Harvesting-Charger IC," *IEEE Transactions on Biomedical Circuits and Systems,* vol. 4, no. 6, pp. 1932-4545, 2010.

[26] C. Peters, J. Handwerker, D. Maurath and Y. Manoli, "A Sub-500 mV Highly Efficient Active Rectifier for Energy Harvesting Applications," *IEEE Transactions on Circuits and Systems,* vol. 58, no. 7, pp. 1542-1550, 2011.

[27] H. Beaudry, "Screen-Printing Piezoelectric Devices," *Proc. 6th European Microelectronics Conference,* pp. 456-463, 1987.

[28] N. M. White and J. D. Turner, "Thick-film Sensors: Past, Present and Future," *Meas. Sci. Technol.,* vol. 8, pp. 1-20, 1997.

[29] A. J. Lovinger, "Ferroelectric Polymers," *Science,* vol. 220, no. 11, pp. 15-21, 1983.

[30] *Piezo Film Sensors Technical Manual Datasheet,* Measurement Specialties Inc..

[31] Z. Cao, J. Zhang and H. Kuwano, "Vibration Energy Harvesting Characterisation of 1cm2 Polyvinylidene Fluoride Generators in Vacuum," *Japanese Journal of of Applied Physics,* vol. 50, no. 9, 2011.

[32] P. Cottinet, M. Lallart, D. Guyomar, B. Guiffard, L. Lebrun, G. Sebald and P. Putson, "Analysis of AC-DC Conversion for Energy Harvesting Using an ELectrostrictive Polymer P(VDF-TrFE-CFE)," *IEEE Transactions on Ultrasonics, Ferroelectrics, and Freuency Control,* vol. 58, no. 1, pp. 30-42, 2011.

[33] D. Vatansever, R. Hadimani, T. Shah and E. Siores, "An Investigation of Energy Harvesting From Renewable Sources with PVDF and PZT," *Journal of Smart Materials and Structures,* vol. 20, no. 5, 2011.

[34] H. Hu, C. Zhao, S. Feng, Y. Hu and C. Chen, "Adjusting the Resonant Frequency of a PVDF Bimorph Power Harvester Trough a Corrugation-Shaped harvesting Structure," *IEEE Transactions on Ultrasonics, Ferroelectrics, and Frequency Control,* vol. 55, no. 3, pp. 668-674, 2008.

[35] *LDT0-028K Piezo Film Sensors Product Datasheet,* Measurement Specialties.

[36] K. Konig and M. Ulrich , "Vibration Energy Harvesting for Process Industry Applications," *ABB AG Corporate Research Center,* 2011.

[37] P. Mitcheson, T. Green and E. Yeatman, "Power Processing Circuits for Electromagnetic, Electrostatic and Piezoelectric Inertial Energy Scavengers," *Microsystem Technologies,* vol. 13, no. 11-12, pp. 1629-1635, 2007.

[38] D. I. Made, Y. Gao, S. J. Cheng, M. T. Tan and M. Je, "Optimum Piezoelectric Energy Harvesting with Buck Boost Circuit in Discontinuous Mode," *International Journal of Information and Electronics Engineering ,* vol. 2, no. 6, pp. 892-894, 2012.

[39] S. Dwari and L. Parsa, "Efficient Low Voltage Direct AC/DC Converters for Self-powered Wireless Sensor Nodes and Mobile Electronics," *Proc. IEEE Telecommun. Energy Conf.,* pp. 1-7, 2008.

[40] J. Sun, D. M. Mitchell, M. F. Greuel and R. M. Bass, "Averaged Modeling of PWM Converters in Discontinuous Conduction Mode," *IEEE Transactions on Power Electronics ,* vol. 16, pp. 482-492, 2001.

[41] *Thinergy MEC202 Thin-Film Micro-Energy Cell Product Datasheet,* Infinite Power Solutions.

[42] H. He, R. Xiong and J. Fan, "Evaluation of Lithium-Ion Battery Equivalent Circuit Models for State of Charge Estimation by an Experimental Approach," *Energies,* vol. 4, pp. 582-598, 2011.

[43] A. V. Ramanan, M. Pakirisamy and S. Williamson, "Advanced Fabrication, Modelling and Testing of a Micro-Photosynthetic Electrochemical Cell for Energy Harvesting Application," *IEEE Transaction on Power Electronics,* 2013.

[44] *LM311 Differential Comparator Datasheet,* Texas Instruments.